Predictive models of mineralogy from whole rock assay data: Case study from Productora Cu-Au-Mo deposit, Chile

Angela Escolme[1], Ron F. Berry[1], Julie Hunt[2,3], Scott Halley[4], Warren Potma[5]

[1]ARC Research Hub for Transforming the Mining Value Chain & CODES, University of Tasmania, Hobart, TAS, Australia, 7001

[2]CODES, University of Tasmania, Hobart, TAS, Australia, 7001

[3]Mineral Deposit Research Unit - Department of Earth, Ocean & Atmospheric Sciences, University of British Columbia, Vancouver, BC, V6T 1Z4, Canada

[4]Mineral Mapping Pty Ltd, 106 Joyce Street, Hawley Beach, TAS, 7307

[5]CSA Global Pty Ltd, Level 2, 3 Ord Street, West Perth, WA, 6005, Australia

Abstract

Mineralogy is a fundamental characteristic of a given rock mass throughout the mining value chain. Understanding bulk mineralogy is critical when making predictions on processing performance. However, current methods for estimating complex bulk mineralogy are typically slow and expensive. Whole rock geochemical data can be utilized to estimate bulk mineralogy using a combination of ternary diagrams and bivariate plots to classify alteration assemblages (alteration mapping), a qualitative approach, or through calculated mineralogy, a predictive quantitative approach. Both these techniques were tested using a dataset of multielement geochemistry and mineralogy measured by semi-quantitative X-ray diffraction data from the Productora Cu-Au-Mo deposit, Chile.

Using geochemistry, samples from Productora were classified into populations based on their dominant alteration assemblage, including quartz-rich, Fe-oxide, sodic, potassic, muscovite (sericite) and clay-alteration, and least altered. Samples were also classified by their dominant sulfide mineralogy. Results indicate that alteration mapping through range of graphical plots provides a rapid and simple appraisal of dominant mineral assemblage in volcanic rocks, which closely matches the measured mineralogy.

In this example, calculated mineralogy using linear programming generated robust quantitative estimates for major mineral phases, including quartz and total feldspars, as well as pyrite, iron oxides, chalcopyrite and molybdenite, which matched the measured mineralogy data extremely well (R^2 values greater than 0.78, low–moderate root mean square error). The results demonstrate that calculated mineralogy can be applied in the mining environment to significantly increase bulk mineralogy data and quantitatively map mineralogical variability. This was useful even though several minerals were challenging to model due to compositional similarities, and clays and carbonates could not be predicted accurately.

Introduction

Mineralogy is a fundamental characteristic for a given rock mass throughout the mining chain, from blasting, through valuable phase extraction to waste management (Hoal, 2008). Understanding mineralogy of the bulk rock, including both the gangue and valuable component, is critical when making predictions on processing characteristics, such as mill throughput or acid generation/neutralization potential (Parbhakar-Fox and Lottermoser, 2015). These characteristics inform important decisions about processing method, mill flow sheet design, mill sizing and waste management strategies. Throughout the exploration and resource development process, mineralogical data are collected mostly in a qualitative manner through the visual logging of rock types and alteration styles. These datasets may be subjective and are commonly inconsistent. Current methods

for quantitative estimates of bulk mineralogy are slow and expensive, particularly where mineralogy is complex and variable.

Traditionally, modal analysis of mineralogy has been done through visual methods such as point counting and image analysis (Pignolet-Brandom and Reid, 1988; Petruk, 1989; Liipo et al., 2004; Donskoi et al., 2007, 2008; Hunt et al., 2008; Lane et al., 2008;). More recently X-ray point counting using SEM-EDS based software has been used widely (Gu, 2003; Fandrich et al., 2007; Lund and Martinsson, 2008; Forrest, 2009; Hoal et al., 2009; Oghazi et al., 2009; Lund et al., 2010). Common commercial packages include Mineral Liberation Analysis (MLA) or Quantitative Evaluation of Minerals by Scanning Electron Microscopy (QEMSCAN). However, these methods are not well suited to the routine analysis of bulk samples at normal assay spacing because they are too slow and expensive. Semi-quantitative X-ray diffraction (QXRD) is a more widely applied method of estimating major minerals (Helle et al., 2005; Knorr, 2010), particularly in the iron ore industry where mineralogy is relatively simple and the process is more readily automated. However, with a nominal detection limit of 0.5 wt % (Omotoso et al., 2006) this method has limited applications when dealing with low abundance minerals, including Cu-sulfides that are commonly detected but poorly quantified. Where mineralogy is complex, the QXRD method is less efficient, as each diffractogram must be manually interpreted for optimum results.

Consequently, quantitative estimates of mineralogy are typically only performed on a small number of ‘representative’ samples and extrapolated to represent large tonnages of rock. Typically, this forms part of a geometallurgy program, whereby samples are chosen to span the perceived range of grade, rock types and alteration styles (Lamberg, 2011; step 2 in Fig. 1). A dilemma exists where the spatial variability of ore, in terms of mineralogy and metallurgical response, must be known to select truly representative samples, but this information is invariably lacking. During scoping and project definition studies, predictions of mine performance are made from the extrapolation of this limited dataset. The most important and risk prone decisions are made during project infancy when the least metallurgy data is available. Early prediction of bulk mineralogy enables more informed variability sampling (Fig. 1, step 2) and provides datasets from which to establish geometallurgical domains and derive mineral processing parameters (Fig. 1, Steps 4 and 5). Predictions of mine performance can be improved where estimates of mineral abundance are extensive (Hunt et al., 2008).

In this paper we present two examples of bulk mineralogy prediction from commonly available whole rock geochemical assay data, using the Productora Cu-Au-Mo deposit, Chile, as a case study. Both approaches are demonstrated for two study sections through the Productora deposit, 6,822,215 mN and 6,820,850 mN, where detailed geological characterization has been established (Escolme, 2016). Across each study section a ‘best estimate mineralogy’ was generated by combining mineralogical data, by QXRD, with geochemical data through a weighted least squares calculation – this best estimate has been used to validate our results against. In order to demonstrate each method of mineralogy prediction, we present the methods, results and a discussion for each. Firstly, we demonstrate a *qualitative* mineralogy estimation approach, referred to as alteration mapping from whole rock geochemistry, using a suite of simple geochemical plots. Secondly, we demonstrate *quantitative* prediction of mineralogy by calculated mineralogy using linear programming.

Deposit Geology

The Productora Cu-Au-Mo deposit is hosted by a hydrothermal breccia complex in the Coastal Cordillera of northern Chile (Fig. 2A). A detailed account of the deposit geology is provided by Escolme (2016). The complex is situated within a thick sequence of Early Cretaceous dacite to rhyolite volcanic rocks that were also intruded by two major stocks; the Cachiyuyito tonalite (129 Ma; Fox 2000) and Ruta Cinco granodiorite (92 Ma) as well as the mineralized Alice granodiorite

porphyry (121 Ma), Zapallo granodiorite porphyry (118 Ma; Fig. 2B) and several phases of dacite and basalt-andesite dykes (Escolme, 2016). The dacite to rhyolite volcanic rocks that host the mineralized breccias are predominantly massive, crystal-rich, lapilli tuffs and review of whole rock immobile element geochemistry shows little compositional variation (Escolme, 2016).

At the camp scale, three significant mineralization and alteration events are recognized; Cachiyuyito sodic-calcic alteration and magnetite-apatite mineralization (on the flanks of the Cachiyuyito stock), Productora breccia complex and Cu-Au-Mo mineralization, and Alice porphyry Cu-Mo mineralization (the latter two are shown in Fig. 2B). This case study is focused on the Productora breccia complex, where brecciation and alteration led to the formation of widespread, complex alteration mineralogy (Escolme, 2016; Fig. 2C, D) Three stages of brecciation and associated alteration have been defined at Productora. Stage 1 produced quartz – pyrite-cemented hydrothermal breccia with muscovite alteration. Stage 2 formed a chaotic matrix-supported tectonic breccia with kaolinite - muscovite – pyrite alteration. Stage 3 tourmaline – pyrite – chalcopyrite ± magnetite ± biotite-cemented hydrothermal breccias are associated with K-feldspar ± albite alteration. Alteration is intense, pervasive and locally texturally destructive. Breccia and alteration boundaries are gradational and stage 3 breccias show significant lateral and vertical variation in cement mineralogy, with deeper regions containing more magnetite, and increasing chlorite after biotite, and pyrite in the south of the complex. Late stage phyllic (illite, chalcopyrite + pyrite) and propylitic (chlorite, epidote, calcite) overprints also occur as discreet veins in the breccia complex and host rocks. Advanced argillic assemblages (quartz – alunite, pyrophyllite – dickite) are observed to the west of the Productora deposit and form a lithocap proximal to the Alice porphyry deposit (Escolme, 2016; Fig. 2B). The proximity of high temperature mineral assemblages and high energy, non-explosive breccia textures (jig-saw fit, clast supported, minor matrix) close to the surface is consistent with a deep level of erosion.

Mineralization is associated with stage 3 breccias (Escolme, 2016). The major hypogene Cu-bearing phase is chalcopyrite. Secondary Cu minerals, including chalcocite, malachite and chrysocolla, have variably developed in the weathering profile across the deposit. The current resource, which includes the neighboring Alice porphyry Cu-Mo deposit, is estimated at 236.6 Mt grading 0.48 % Cu, 0.10 g/t Au and 135 ppm Mo (Hot Chili Ltd, 2016).

Weathering is variable but generally limited across the Productora deposit. The weathered profile typically extends to between 80–100 m depth leading to oxidation of sulfides and formation of clay minerals. Within the profile, total clay content (including smectites and kaolinite) is typically between 6–12 wt %, but locally exceed 20 wt % (based on QXRD data). Narrow domains of deeper weathering, to 200–350 m, occur throughout the deposit and coincide with fault zones. There are two major fault orientations at Productora: a north-trending set which control the orientation of the breccia bodies, and a northwest-trending set, which cross cut the north-trending set and displace mineralization (Ray and Dick, 2002; Beeson 2012).

Data

Whole rock geochemistry data

Standard assay protocols for drilled samples at Productora include analysis of 33-elements by inductively coupled plasma-atomic emission spectrometry (ICP-AES) on every 1 m assay interval. Reverse circulation and whole core samples used in this study were submitted to ALS Global Ltd laboratories, La Serena, Chile. Prepared samples underwent near-total digestion by four acids (HNO_3-$HClO_4$-HF-HCl digestion and HCl leach) and the resulting solution was analyzed by ICP-AES (ALS, 2018). In this study, assay data from 1,642 samples from 26 drill holes across two cross sections are used.

QXRD

A total of 625 laboratory pulp reject samples were selected from two study sections to generate a measured bulk mineralogy training data set. Samples were submitted to Genalysis Laboratory Services Pty Ltd., Perth, Australia, for QXRD analysis. Sub-samples of approximately 20 grams were crushed to an average particle size of 4 µm and prepared as un-oriented powder mounts. X-ray diffraction (XRD) patterns were generated on a PANalytical Cubix3 XRD fitted with a PIXCEL solid state detector and copper radiation (operating at 45 kV and 40 mA). The XRD apparatus was configured with a graphite monochromator in the diffracted beam and fixed slits. Qualitative analysis was performed using the Bruker Diffrac.EVA 3.2 Search/Match software with the ICDD PDF-2 (2011) database. Rietveld quantitative phase analysis, for crystalline phases only, was performed using SIROQUANT® Version 4 software (S. Ness, pers. commun. 2014). The detection limit was 0.5 wt %, with absolute errors as in Table 1. Clay mineralogy for nine samples was confirmed by clay separation, followed by measurement of oriented clay mounts prepared by air drying, glycolating and heat treatment (E. Lebedeva, pers. commun., 2014).

Combining QXRD mineralogy with whole rock assay data

In order to overcome some of the limitations of QXRD analysis that ensue with low mineral abundances, QXRD data can be combined with chemical assays through a weighted least squares calculation following the methods of Berry et al. (2011) using the 'NNLS' subroutine of Lawson and Hanson (1995). A detailed method description and calculation workbook (WLSQ-COMBI_v1.xlsm), including minerals and mineral compositions used in this case study, are provided in the Digital Appendix. This method aims to find the modal mineralogy that is consistent with chemical analysis and is also as close as possible to the QXRD results. This is achieved using the non-linear Solver routine in Microsoft Excel™ to minimize the sum of normalized residuals (excess chemistry or mineralogy) squared through varying the predicted abundance of each mineral. The method enables a complex and broad range of minerals to be robustly estimated, with high abundance minerals determined by QXRD measurements and low abundance minerals estimated from the chemical assays.

Comparison of the weighted least squares corrected QXRD data (WLSQ) against the raw QXRD data can be used to identify phases that have abundances close to QXRD detection limits. Minerals present in high abundance, such as quartz, feldspars, micas and clays show good correlation between QXRD and WLSQ (Fig. 3). A breakdown in the correlation between QXRD and WLSQ at high K-feldspar values (Fig. 3B) likely reflects an issue with analysis of K when present at high values. The Chi-squared measure of fit indicates that a modal mineral composition can be calculated for 95% of the samples that is compatible with both the QXRD data and the chemical analysis at better than 5% confidence level (65% of samples gave a calculated mineralogy that fitted both QXRD and the chemical analysis at better than 50% confidence level). For lower abundance phases, the correlation between QXRD and WLSQ is poor (Fig. 3K-L). This is predominantly due to the high detection limits associated with the QXRD method (Omotoso et al., 2006). For example, in the Productora dataset, molybdenite was rarely detected by QXRD, but Mo is present in the chemical analyses (ore reserves include 166.8 Mt @ 151 ppm Mo, Hot Chili Ltd., 2016). Where molybdenite is detected by QXRD, it is predominantly overestimated relative to the concentration of Mo detected by chemical assay (Fig. 3L). As there is only one known Mo-bearing phase in the deposit, the WLSQ result calculated from assay is a better representation of the abundance of molybdenite at Productora than the QXRD. This is largely because the detection limit for Mo in the multielement geochemical assays (1 ppm or 0.0001 %) is much lower than the QXRD detection limit for its mineral host, molybdenite (0.5 wt %). Similarly, chalcopyrite is poorly represented by QXRD due to its low abundance and the high detection limit.

Measured mineralogy results

In this study, WLSQ data from the two study sections is used as a training set for calculated mineralogy and to provide a frame of reference to review the two approaches to predicting bulk mineralogy. An overview of the WLSQ dataset indicates that altered volcanic rocks at Productora are dominated by quartz, K-feldspar, albite and illite-muscovite (Fig. 4). Quartz content is typically between 20 and 42 wt %, but ranges up to 88 wt % and is typically higher in samples from the northern section. Albite is significantly more abundant (mean 15-20 wt %) than calcic plagioclase, which has mean values of <5 wt % for both study sections but locally occurs up to 62 wt %. Amphibole, chlorite, Fe-oxides, pyrite, and tourmaline are typically below 10 wt % with some far outliers. Biotite varies considerably between the two sections, being much more abundant (mean 5 wt %) in the south with far outliers up to a maximum of 40 wt %.

Pyrite is the most abundant sulfide and chalcopyrite was the most commonly detected Cu-Fe sulfide phase, although it was below detection limit in 401 of the QXRD analyses. Kaolinite is the most common and abundant clay in the sample set, followed by montmorillonite. Vermiculite, a mica-group mineral, is rare. Calcite is the most common carbonate mineral, although ankerite was detected in 48 samples by QXRD. The sulfates anhydrite, jarosite and gypsum were detected in 49, 41 and 32 samples respectively. Since anhydrite and gypsum cannot be distinguished using the chemical assays available they are reported together from here forward.

Overall, the major mineralogy of samples from the northern section (6,822,215 mN) is elevated in quartz, K-feldspar, muscovite, tourmaline and kaolinite relative to the southern section (6,820,850 mN), where there are higher abundances of total plagioclase, biotite, chlorite, pyrite, amphibole and calcite (Fig. 4).

Alteration mapping from whole rock geochemistry

Multielement geochemistry is typically collected during the exploration phase, although increasingly as routine on all samples. Variations in major mobile element chemistry can be used to quickly identify dominant alteration assemblages whereas immobile elements can be used as lithogeochemical discriminators. Identification of alteration styles and rock type from both soil, rock chip and drill core samples have been used to aid exploration activities at deposit and district scales (e.g. Yerington, Halley et al., 2015; and North West Province, Zambia, Halley et al., 2016). Classification of samples based on geochemistry is powerful when combined with traditional field techniques — especially when working in highly altered rocks where logging may be inconsistent. Sample classification by geochemistry is also useful in the mining environment as it provides a simple and rapid approach to mineralogical domain definition, with bulk data processed using commonly available software. These basic classifications can provide insights into mineralogical variability at a deposit scale which may then inform sample selection for metallurgical test work.

Since Productora is hosted by a thick package of volcanic rocks with limited compositional variability in the primary host rock (predominantly dacites to rhyodacites with late cross cutting intermediate to mafic dykes) but with discreet alteration styles (Fox, 2000; Ray and Dick 2002; Escolme, 2016), the deposit provides a suitable dataset to demonstrate alteration classification from geochemistry in a calc-alkaline volcanic rock hosted, porphyry-related system. In addition, the availability of a large dataset of QXRD measurements makes Productora an ideal case study to review and validate this approach.

Alteration mapping method

The following method describes the use of several geochemical plots which can be used to manually discriminate dominant sample mineralogy, with a brief explanation of the rationale behind each plot using data (including measured mineralogy) from the Productora deposit to demonstrate. The

intention of this approach is to provide a simple and rapid method of defining domains of discreet alteration, ultimately at the discretion of the analyst and their interpretation of the dataset. The methodology presented here includes the classification of: least altered samples, quartz-rich samples and major alteration assemblages including magnetite, sodic (albite), potassic (K-feldspar, biotite), sericite (muscovite) and clay-alteration. The workflow for this case study is summarized in Figure 5. It should be noted that in the case study presented weathering is not extensive and samples from the weathering profile were not considered separately. Where weathering is intense and extensive, consideration should be given to geochemical trends that may result from variable cation mobility in the weathering profile. It should also be noted that discrimination between supergene and hypogene clay is not discussed here, although spatial distribution and mineral associations (e.g., hypogene sulfides) should be used as a guide. Sample classification as described should be performed on each rock type separately – rock type may be informed by logging or review of immobile element geochemistry (e.g., Halley et al. 2016). Classification groups should be based on natural populations inherent to the dataset rather than fixed fields, the use of point density contours can provide a useful tool to identify these group on plots for large datasets. Since this is a manual approach, classification is somewhat subjective to the analyst – although it is acknowledged that applying a statistical framework to such classifications would improve consistency and repeatability. Classification of samples is an iterative process whereby samples may be reclassified several times as they are reviewed using different plots, until the most appropriate classification is determined — ultimately at the discretion of the analyst.

Least altered samples

At Productora, mineralogical variability across the deposit is primarily the result of intense hydrothermal alteration associated with brecciation and mineralization. The least altered samples are typically late stage intrusions or the most distal samples. Sodic and potassic alteration leads to deviations in major element geochemistry toward Na-rich or K-rich compositions relative to unaltered host rocks. Data from the two study sections at Productora were plotted on a Ca-K-Na ternary plot (one rock type at a time) in order to identify samples that may be considered least altered, i.e., plotting close to the expected composition of the rock type (Fig. 6). Samples that were interpreted as least altered based on their geochemistry, largely correspond with the Zapallo post-mineralization granodiorite intrusion or mafic dykes which show little to no visible alteration.

Estimation of quartz abundance

Silicon is not included in routine exploration geochemical analysis suites as Si analysis is not possible after a four acid digestion. Since Si is a major component of many rock samples, particularly in the porphyry environment, SiO_2 can be crudely estimated as the difference between the sum of other major element oxides and 100 percent. Whilst this estimate does not take into consideration loss on ignition (LOI), which may be significant in carbonate or clay-rich rocks, it can provide a useful proxy guide for quartz abundance in appropriate environments (e.g., Cobeñas and Halley, 2015). Using the method described above, SiO_2 was estimated from the Productora geochemistry dataset and compared to SiO_2 estimated from the WLSQ mineralogy (sum of SiO_2 in each mineral for each sample; Fig. 7A). Overall the data are well correlated (R^2=0.80), but the relationship breaks down at lower values of SiO_2 (< 60 wt %), where variability is on average 8 % with outliers up to 25 %. At high estimated SiO_2 abundance (>75 wt % SiO_2), the correlation of measured quartz (WLSQ) and calculated SiO_2 is good, although not one-to-one (Fig. 7B). Using SiO_2 estimated from geochemistry, samples with far outlying values of SiO_2 (for each rock type) were classified as ‘high quartz’. In this example most of the samples that plotted at anomalously high SiO_2 values were rhyolite samples. Review of other available WLSQ data indicates that, in general, samples with high quartz also contain high muscovite but low total clay and K-feldspar compared to other samples (Fig 7C, 7D, 7E), which is consistent with a phyllic alteration assemblage rather than just protolith composition.

Magnetite alteration

Mobilization of Fe requires highly saline and oxidized hydrothermal fluids (Burnham, 1979). In the porphyry environment, Fe along with other base and precious metals, are typically sourced from magmatic fluids (Clark and Arancibia, 1995; Hemley et al., 1992; Whitney et al., 1985). In IOCG systems, evaporitic or metamorphic saline fluids may also contribute to the mobilization and transport of large quantities of Fe (Barton, 2014).

Immobile elements Sc and V both substitute for Fe in the lattice of silicates, such as amphiboles and pyroxenes, and typically occur in a ratio of 8:1 respectively in the bulk geochemistry of unaltered volcanic rocks. Vanadium partitions strongly into magnetite whereas Sc only has weak affinity for magnetite (partition coefficients up to 54 and 3.3 respectively; Luhr and Carmichael, 1980). It can be inferred that igneous rocks with high V/Sc are likely to have undergone Fe-addition. In the Productora dataset presented here, samples that fall above the expected 8:1 ratio for V:Sc also span to higher Fe/Al and Fe/K ratios than the majority of the data (Fig. 8A and 8B), which QXRD data indicates is dominantly hosted in Fe-oxides (Fig. 8C). Compared to the broader Productora dataset, which typically contains ~2.5 wt % Fe, samples with high V:Sc contain >6 wt % Fe and plot far from the pyrite Fe-S ratio (Fig. 8D) indicating that pyrite is not the dominant Fe-hosting mineral and Fe-addition occurred. Geological logging validates that these samples contain abundant Fe-oxide – typically as magnetite. Samples identified as high in Fe also show elevated amphibole and apatite (Fig. 9), which is consistent with other magnetite mineralization occurrences in northern Chile (Ménard, 1995).

Feldspar alteration mineralogy

Feldspar minerals make up a significant proportion of mafic to felsic igneous rocks, typically 50-70 wt % (Le Maitre, 1989). Hydrothermal alteration leads to the modification of primary feldspars, as well as other silicate minerals. Hydrothermal alteration commonly leads to the addition of K (potassic alteration) and/or Na-Ca (sodic-calcic alteration) which leads to the predominance of orthoclase and/or biotite, and albite respectively. Phyllic alteration is characterized by the conversion of feldspars to sericite (muscovite, illite, phengite) whereas argillic alteration leads to the formation of clay (kaolinite).

Major element geochemistry provides a proxy for the predominant alteration minerals present. Alkali-(Na, K) alumina molar ratio plots (Davies and Whitehead, 2006) can be used to rapidly classify samples by their dominant mineralogy (e.g. Halley et al., 2016; Cobeñas and Halley, 2015). To demonstrate this, samples with both whole rock geochemistry and mineralogy measured by QXRD were plotted on the Na-K molar ratio diagram and colored by measured mineral abundance for K-feldspar (Fig. 10A), albite (Fig. 10B) and muscovite (Fig. 10C). Samples with the highest measured abundances of these minerals are seen to plot closest to the pure mineral composition on the diagram, indicating that whole rock geochemistry can be used as a useful proxy for predominant mineralogy. Productora data for altered samples (excluding those samples already classified as least altered, quartz-rich and Fe-oxide altered) were plotted on the Na-K molar ratio plot. Point density contours (Fig. 10D) indicate that high data concentrations are associated with muscovite-rich and K-feldspar/biotite rich compositions. Whilst biotite is present at the deposit, review of a K/Al against (Fe+Mg)/Al plot indicated that for samples that plot at the K-feldspar/biotite node, biotite is always subordinate to K-feldspar. Data populations were manually classified into eight classes of dominant alteration mineralogy; K-feldspar, muscovite, K-feldspar-muscovite, albite, albite-muscovite, alkali-feldspar (mixture of K-feldspar and albite), alkali-feldspar-muscovite and argillic (Fig. 10E). Review of this classification against measured mineralogy provides validation of the results (Fig. 11).

Sulfides

Where sulfide mineralogy is simple and well understood, bulk geochemistry can be used to discriminate dominant sulfide mineralogy. Within the Productora WLSQ dataset, sulfide mineralogy predominantly consists of pyrite (0-12.6 wt %) and chalcopyrite (0-1.72 wt %), with lesser supergene chalcocite (0-0.20 wt %) and minor molybdenite (0-0.04 wt %). Samples with both geochemistry and measured mineralogy by WLSQ (n=625) were plotted on a Cu-Fe-S ternary diagram and classified by the abundance of pyrite (Fig. 12A), chalcopyrite (Fig. 12B), chalcocite (Fig. 12C) and non-sulfide Cu minerals (Fig. 12D). Samples which contain the most pyrite plot close to the bulk Cu-Fe-S composition of pyrite on the Fe-S axis (Fig. 12A), whereas samples high in chalcopyrite plot closer to the compositional Cu-S tie line for chalcopyrite (Fig. 12B). Similarly, samples high in chalcocite plot about the chalcocite tie-line (Fig. 12C). Samples containing Cu in predominantly non-sulfide minerals plot on the Fe-Cu axis, with low to no S content (Fig. 12D).

Plotting all the data from the two study sections onto the Cu-Fe-S ternary plot and contouring by point density indicates that many of the samples are barren (<0.05 wt % Cu) but a significant number of barren samples also contain high pyrite — these samples plot along the Fe-S axis toward the composition of pyrite with low Cu/Fe (Fig. 12E). Using this approach, samples can be quickly classified by their dominant Cu-Fe-sulfide mineralogy into the following populations: barren (low Cu/S and low Fe/S), pyrite-, chalcopyrite-, chalcopyrite-pyrite-, chalcocite-rich and those containing non-sulfide Cu (Fig. 12F). In this case study, classification by this approach was validated against QXRD data (Fig. 13). It should be noted that classification via a ternary plot is based on ratios not absolute values. Consequently, on the ternary diagram it is not possible to distinguish between samples with high abundance or low abundance. Some samples which are classified as pyrite-dominant may in fact only contain a very low abundance of pyrite (as indicated in Fig. 13). It is recommended that after classification using the Cu-Fe-S ternary plot, absolute Cu and S values are reviewed in order to determine the abundance of sulfide (assuming no other significant S-bearing phases are present).

Alteration mapping results

A total of 1,642 samples were classified for dominant alteration mineralogy and dominant Cu-Fe-sulfide species based on multielement geochemistry using a variety of graphical plots including major element ternary plots, bivariate plots and an alkali- (Na, K) alumina molar ratio plot. Modal mineralogy, determined by QXRD, was available for 625 of these samples which enabled the methods to be validated. Classified samples were plotted on cross sections and validated against graphic logging and core photography. Alteration domains and domains of dominant sulfide species were interpreted for each section (Figs. 14-17). Discrete domains of variable alteration mineralogy, on a scale relevant to mining, can be identified from the classified data. The two sections, from opposite ends of the deposit, show markedly different alteration mineralogy. Section 6,822,215 mN has significant muscovite, kaolinite and quartz-muscovite alteration to the east. These acid alteration assemblages are juxtaposed against K-feldspar dominant assemblages which transition to alkali-feldspar and muscovite assemblages to the west. In the south on section 6,820,850 mN, little acid alteration is observed but there is more albite and mixed alkali feldspar ± muscovite alteration. Domains of least altered samples on section 6,820,850 mN coincide with the post-mineralization Zapallo granodiorite intrusion and rhyodacite host rocks in the West.

Sulfide mineralogy also shows significant variability across the deposit (Figs. 16 and 17). Compared to the southern section, the northern section (6,822,215 mN) shows more variation in dominant sulfide assemblage over short distances (20 m). The northern section also has more abundant chalcopyrite relative to pyrite at depth. Classification of section 6,820,850 mN data indicates that pyrite dominates at depth, and more broadly across the section, whereas chalcopyrite is more abundant in shallower

portions of the deposit. The data also indicates that significantly more non-sulfide copper occurs in the upper 100 m of this section compared to the northern section.

Alteration mapping discussion

Using multielement geochemical data, samples from two sections of the Productora deposit were classified for dominant alteration mineralogy and dominant Cu-Fe-sulfide species. Compared to measured mineralogy, established by QXRD, the methodology of discrimination by geochemical plots provides a robust estimate of dominant mineralogy. The method is also rapid — data can be interpreted in minutes, and incurs no additional costs outside of the license for appropriate geochemical software provided the geochemical data is available. A significant limitation of the methods outlined here is that they cannot be universally applied to all environments. For example, weathered samples may show variable loss of major elements causing classifications to be skewed. In this example, the hosts rocks are from a calc-alkaline volcanic arc sequence with porphyry-style alteration. Geochemical alteration trends are inferred from established unaltered rock compositions available in the literature. In the case of sedimentary environments, an unaltered protolith composition would need to be established as a baseline.

The classifications determined in this example provide a basis for broad domains of variable mineralogy to be established. These domains provide a simple model for mineralogical variability that may inform metallurgical sampling programs or give context to existing samples. However, the data is categorical and qualitative, not quantitative. A quantitative prediction method, calculated mineralogy by linear programming, is outlined below.

Calculating modal mineralogy from whole rock geochemistry

Calculated mineralogy method

Modal mineralogy can be calculated from chemical assay data through linear programming and the Simplex method (Press et al., 1986) using Solver in Microsoft Excel™ (Berry et al., 2011; Berry et al., 2015). A major benefit of the linear programming method is that there is no practical limit to the number of minerals considered. In addition, non-negativity can be enforced, unlike alternative simple least squares models (Bryan et al., 1969; Le Maitre, 1981; Paktunc, 1998, 2001) that require more chemical constraints than calculated mineral phases. In most cases, simple least squares models allow the calculation of negative mineral abundances, although this provides an additional measure of the fit quality and warns the user that the mineral species selected are incompatible, such results are physically impossible. Examples of the application of linear programming to solving modal mineralogy include the methods of Braun (1986) and Podkovyrov et al. (2003). The work of Braun (1986) is largely focused on resolving mineral composition in a simple three phase system and determining maximum and minimum abundances with additional constrains provided by QXRD. Podkovyrov et al. (2003) apply linear programming to normative mineral decomposition of sedimentary rocks and calculate up to 17 minerals. Both of these approaches are not suitable to resolve the complex range of minerals or volume of samples that an ore deposit presents.

A list of minerals present and their compositions must be provided for linear programming to be applied. The mineral compositions may be determined either by analysis (e.g., electron microprobe) or chosen from the literature. In this example both these approaches were used, the mineral list and compositions used are provided in the Digital Appendix workbook (ASSAY2MIN_v1.xlsm). A training set of known mineralogy is also required, which can be established through QXRD (as in this study) or other independent methods (e.g., SEM, point counting). For a deposit scale application, a

training set of several hundred samples is recommended, however this number is subject to the complexity and variability of the individual deposit since the training set must represent the variability in mineralogy. A detailed description of the calculated mineralogy by linear programming method applied at Productora and a macro-enabled workbook for the calculation (ASSAY2MIN_v1.xlsm) is provided in the Digital Appendix. A brief outline is provided below.

For this application, the linear programming method (also known as linear optimization) aims to maximize a linear objective function based on the proportional sum of a 'property value' of each mineral listed, whilst minimizing the residual element abundances for a given modal mineralogy estimate. This requires user input in order to optimize the property values for each mineral. The property value acts as a proxy for the likelihood of the mineral occurring, with higher values for common minerals and low or negative values for rare minerals. Independent geological information (measured by QXRD or SEM point counting) on the mineralogy is required for the mineral list and these property values to be set correctly. In this case the 625 sample QXRD training set corrected against chemical assay by weighted least squares (method described above and in Digital Appendix) was used to train the model and establish appropriate property values. Calculated mineral abundances are limited to $\geqslant 0$ % and $\leqslant 100$ % in order to ensure results are physically possible. Additional constraints can also be applied to limit upper mineral abundances as required. The linear program used was the "Simplex LP" model from the Solver add-in available in Microsoft Excel™. Using a suitable mineral list and compositions appropriate for the Productora deposit, an Excel™ macro enables the automatic calculation of mineralogy from a large number of analyses. The optimization is derived by a manual method. The parameters were set to maximize accuracy of the calculation for the most abundant minerals, in this case quartz and feldspar components. Elements that are uniquely allocated to a single mineral always give a good result.

Calculated mineralogy results

Modal mineralogy for Productora was calculated for a list of 38 minerals by linear programming using the 15 most abundant elements reported from a four acid digest and ICP-AES dataset (Al, As, Ba, Ca, Cu, Fe, K, Mg, Mn, Mo, Na, P, S, Ti and U). Overall, the most robust calculated mineralogy results were returned for the major mineral components quartz and total feldspars (R^2 values greater than 0.8 and low RMSE; Fig. 18 and Table 2). Other minerals which show a strong correlation (R^2 >0.6) but a larger RMSE include pyrite, iron oxides, chalcopyrite, titanite+rutile and apatite. Molybdenite results returned excellent correlations and RMSE, owing largely to its distinctive chemistry compared to other low abundance minerals found at Productora (Table 2). For the sample population and number of variables, R^2 is the same as adjusted R^2 to two significant figures.

The correlation between calculated muscovite, biotite and chlorite results with the WLSQ data is poorer (R^2 <0.5, moderate–high RMSE; Table 2) due to compositional similarities between these minerals, particularly between biotite and chlorite which results in one mineral being made at the expense of the other in the numerical models. Thus, it is preferable to interpret the sum of these minerals (total chlorite and micas) rather than the individual minerals (Fig. 18G; $R^2 = 0.48$). Despite these challenges, the numerical modelling results provide a good indication of the range in the abundance of chlorite and mica, which is important in geometallurgical applications as these phyllosilicate minerals can cause problems for flotation when present in high (> 30 wt %) abundance (Berry et al., 2013).

Clay minerals proved particularly challenging to numerically model and produced poor results overall, with correlation coefficients of <0.1 and high RMSE values (Table 2, Fig. 18H). Calculations tend to either radically over-estimate clay content at the expense of feldspars and mica, or under-estimate clay. This problem was addressed by applying upper limits (7 wt %), informed by the measured training dataset, to the amount of each clay mineral allowed in the modelled results.

Other minor minerals which were challenging to numerically model include carbonate minerals (calcite, ankerite and dolomite) and anhydrite/gypsum. This is largely due to their chemistry and because no data was available for volatile phases in the ICP-AES database. Similarly, tourmaline, amphibole, epidote and jarosite all proved difficult to predict due to their similarities in major element chemical composition to other minerals, the lack of boron analyses in the case of tourmaline.

Spatial comparison of the results for significant mineral phases, including total quartz and feldspar, total chlorite and micas, pyrite and total clays (Figs. 19-22), against WLSQ data, demonstrates that the results calculated by linear programming show a similar distribution to that of the measured mineralogy. Our experience is that this method will produce a good result for 98% of unknown samples. The remaining 2% are typically samples that were not adequately represented in the training data. The method is suitable for predicting deposit-wide variations in mineralogy. The mineralogy for individual samples that diverge from the deposit trends need to be confirmed by direct measurement.

Spatial variability in mineralogy at Productora

The linear programming model (LP) was applied to the deposit wide dataset in order to calculate mineralogy on every multielement assay interval. The deposit-wide distribution of total quartz and feldspar, total chlorite and micas, pyrite and total clay calculated by the LP method for each assay interval were then modelled as 3D shells using Leapfrog Geo® version 3.1.0 interpolant function, with modelling parameters outlined in Table 3. Plan slices from the 3D model are presented in Figures 23 and 24.

The 3D model of total quartz and feldspar indicates that the north-eastern portion of the open pit design contains higher (significant domains > 70 wt %) total quartz and feldspar than the southern portion (< 70 wt %; Fig. 23A-C). In the northeast, total quartz and feldspar content decreases with depth from predominantly >70 wt % to <70 wt %.

Total chlorite and mica content is extremely variable across the deposit, ranging from <10 wt % to >25 wt % over narrow intervals (10s of meters; Fig. 23D-F). The total chlorite and mica content broadly increases toward the south and with depth. Larger domains of >25 wt % total chlorite and mica were modelled in the southern part of the pit design. Domains of elevated total chlorite and mica (>20 wt %) are also predicted on the eastern side of the deposit. The distribution of total chlorite and micas is somewhat antithetic to the total quartz and feldspar.

Pyrite abundances varies widely across the deposit (<0.1 wt % to > 6wt %; Fig. 24A-C). Generally, pyrite content increases with depth and toward the southeast. There are discrete zones where pyrite exceeds 6 wt %. These domains are both laterally and vertically continuous over 100s of meters.

Despite the poor correlation between measured and modelled clay abundance, the calculated mineralogy results show broad trends that may inform selection of samples for further test work. Modelled clay abundance across the deposit generally decreases from >7.5 wt % in the upper 100 m from surface, to <2.5 wt % below 120 m depth (Fig. 22D). This is consistent with the broad weathering profile at Productora. The interpolant of the modelled total clays indicates that several clay-rich (>7.5 wt %) domains are also predicted at depth (680 m RL) within the pit design, including one in the north-east and one in the south (Fig. 24D-F).

Calculated mineralogy discussion

Application of calculated mineralogy as a method for estimating modal mineralogy

Results from this study indicate that calculated mineralogy through linear programming using the method of Berry et al. (2011) provides a useful estimation of modal mineralogy from chemical assay in quartz-feldspar dominant assemblages. However, the calculated mineralogy methods fails to accurately quantify minerals where ambiguity between minerals exists due to similarities in chemical

composition, particularly between clay minerals and feldspar (both dominated by Al and Si), carbonates and other Ca-rich minerals, and ferromagnesian minerals. Carbonate predictions may be improved through inclusion of additional analyses, such as loss on ignition (LOI) data, CO_2 and also SiO_2 (Berry et al., 2015). Tourmaline is a significant phase in this example with relevance to geometallurgy, owing to its hardness and high abrasion characteristics (Dana and Hurlbut, 1971). In the current study, its abundance has been poorly estimated due to the lack of boron assay data and the similar major element composition of tourmaline to amphiboles and other mafic minerals. However, other geological proxies for tourmaline distribution within the ore body exist at Productora since tourmaline is strongly associated with K-feldspar alteration and elemental Cu grade. A significant limitation of the calculated mineralogy method is that an appropriate training set of known mineralogy is critical to model success. The model(s) are only accurate for mineral compositions similar to those of the training set used in model development. Mineral compositions falling outside of this range are unlikely to be predicted correctly.

Application of calculated mineralogy to geometallurgy

This research provides a new case study demonstrating the potential to translate chemical assays to complex mineral proportions on a deposit-wide scale amenable to the mine planners. The calculated mineralogy method enables chemical assay data to be transformed into tangible information about rock character for further modelling, or as a foundation to inform the sampling and test work of a geometallurgy program. The ability to generate quantitative predictions of major mineral proportions on every assay interval is a significant advantage in the field of geometallurgy, as it provides a quick and cost effective method to increase mineralogical data by many orders of magnitude. In this example 625 QXRD analyses have been transformed into 133,963 estimates of mineral abundance, significantly enhancing the potential for modelling the geometallurgical characteristics of the Productora deposit.

Understanding mineralogy across a deposit is fundamental to any mining feasibility study (e.g. Hoal, 2008). In many hydrothermal ore deposits, particularly porphyry deposits, quartz and the feldspars are the most common hard minerals (7 and 6 – 6.5 on Mohs hardness scale respectively; Dana and Hurlbut, 1971). They are likely to have significant impact on mill throughput when abundant in the ores (e.g. Montoya et al., 2011). Having knowledge of the variability in total quartz and feldspar across a deposit at an early stage, in this case pre-feasibility, ensures comminution sampling covers the range of rock and alteration types and thus expected rock strengths (ease of crushing, grinding etc.). This enables samples to be appropriately weighted in process model simulations by how representative they are. In this example the 3D model of total quartz and feldspar indicates that the shallow northern half of the open pit design contains more quartz and feldspar (locally >80 wt %) than the southern portion (Fig. 23). It is inferred that these rocks are likely to be harder in the near-surface in the north, which will lead to higher comminution costs, and reduced throughput whilst mining these domains compared to other parts of the deposit.

Pyrite is a major contributor to acid rock drainage and in high abundances can cause dilution of any metal-bearing concentrate produced from the ore. This study has shown that it is possible to make robust predictions of its occurrence and distribution throughout a deposit using calculated mineralogy (Fig. 18D). At Productora, pyrite abundance increases with depth, particularly in the south, and locally there are discrete zones of >6 wt % pyrite (Fig. 24). This pyrite model will provide a key dataset to enable pyrite content, of both ore feed and waste rocks, to be accurately predicted throughout the project life.

Clay minerals can have significant impact on flotation when they occur in high abundance (Farrokhpay and Bradshaw, 2012; Cruz et al., 2013; Farrokhpay and Ndlovu, 2013). Using the calculated mineralogy results it was possible to broadly estimate areas of high abundance clay and

other phyllosilicates at Productora. Significant domains of high (>25 wt %) total chlorite and mica were identified in the south of the pit design (Fig. 23).

Modelled clay abundance across the deposit is higher (>7.5 wt %) within 100 m of the surface (Fig. 20 and 22) and generally decreases with depth. This largely corresponds with degree of weathering, as recorded in Hot Chili Ltd.'s drill core logging database. However, there are also several clay-rich domains at depth, including one in the north-east and one in the south (Fig. 24). A review of logging results from these areas has validated the modelled clay. In the north-east the clay domain is associated with hypogene kaolinite observed in the clay-rich Habanero ore zone (Escolme, 2016). In the south, the clay domain has been logged as a weathered zone where intersected by drill core (Hot Chili Ltd geological logging). These examples highlight the potential applications of the calculated mineralogy model, particularly when combined with other available data. The calculated mineralogy method provides the ability to rapidly assess the deposit for mineralogical variability and facilitates the identification of discrete zones which are anomalous or require additional test work to ensure that all mineralization and alteration types are suitably characterized.

Despite the obvious advantages of using calculated mineralogy for geometallurgy, there are only limited examples available in the literature. Comparable examples of the development, and application of a complex deposit-scale calculated mineralogy were limited in the literature at the time of writing. At the La Colosa deposit, Colombia, calculated mineralogy was used successfully for class-based analysis facilitating the development of predictive proxy support models of comminution indices (Montoya et al., 2011). Clearly there is scope for much greater utilization of calculated mineralogy as a method of predicting modal mineralogy, both across a given deposit and for niche applications. This technique may be integrated into geometallurgical studies if the predicted mineralogy is correlated with metallurgical properties; and once trained models may be automated for routine application to large datasets.

Summary

Mineralogy is a fundamental characteristic for a given rock mass throughout the mining value chain and understanding bulk mineralogy is critical when making predictions on processing performance. A major challenge in current practice is that estimating bulk mineralogy is typically slow and expensive, particularly where mineralogy is complex and variable. Consequently, quantitative estimates of mineralogy are typically only performed on a small number of samples – with little evidence to determine if they are truly representative. In this paper we have presented two methods of bulk mineralogy estimation using whole rock multielement geochemical data – which is becoming increasingly common in company datasets. Both methods were applied to a dataset of multielement geochemistry and a dataset of combined assay data with QXRD, from two sections through the Productora Cu-Au-Mo deposit.

The first method classified samples by their dominant alteration mineralogy based on simple geochemical discrimination plots. Discrimination by geochemistry is particularly amenable to the mining environment in that it provides a simple and rapid approach to sample classification, with bulk data processed using commonly available software. In this example, samples were classified into groups of least altered, quartz-rich and major alteration assemblages including Fe-oxide, sodic, potassic, muscovite (sericite) and clay-alteration. Samples were also classified by their dominant sulfide mineralogy. Classifications were validated against assay data combined with QXRD (WLSQ) measured mineralogy, which demonstrated that classified groups were dominated by the expected mineralogy. The estimated mineralogy was plotted on cross sections which revealed discrete domains of variable alteration mineralogy on a scale relevant to mining. Results indicate that on the northern section, acid alteration assemblages (muscovite - kaolinite - quartz) in the east are juxtaposed against K-feldspar dominant assemblages which transition to alkali-feldspar and muscovite assemblages in the west with variable proportions of pyrite to chalcopyrite. The southern section has more albite and

mixed alkali feldspar ± muscovite alteration with significant least altered domains, which coincide with the post-mineralization Zapallo granodiorite intrusion. Shallow non-sulfide Cu is more abundant in the south and pyrite dominates at depth.

The second method demonstrates quantitative estimation by calculated mineralogy using the linear programming and the Simplex method (Press et al., 1986) with Solver in Microsoft Excel™ (Berry et al., 2011; Berry et al., 2015). The QXRD data was used as a training set to develop a model to fit 38 mineral compositions to the multielement assay data from Productora. For this example, the results of the mineralogy calculations are best for the major minerals (quartz and feldspar; R^2 >0.78, low RMSE) and strong for several other significant minerals including pyrite, iron oxides and molybdenite matching the preferred value extremely well (R^2 >0.7, low–moderate RMSE; Table 2). The results reveal significant variation in the proportions of quartz and feldspar, micas and chlorite, pyrite and clays occurs across the study sections and the Productora deposit. Several minerals, including clays and carbonates, were challenging to model due to their compositional similarities to other minerals. Additional analytical data is required in order to more accurately constrain their proportions in the calculation — this is an area recommended for future work. Since the results are quantitative they enable mineralogical variability to be investigated at the meter scale (i.e., the assay interval) which can in turn provide context to metallurgy test work or inform further sampling. The quantitative numerical data is also amenable to further modelling or inclusion in a block model.

Acknowledgements

This research was conducted by the ARC Research Hub for Transforming the Mining Value Chain (project number IH130200004), with support from Hot Chili Ltd, Commonwealth Scientific and Industrial Research Organisation, Society of Economic Geologists and Australasian Institute of Mining and Metallurgy. This work was part of a PhD study and the lead author extends their gratitude to David R. Cooke who was the primary supervisor. We also thank the Hot Chili Ltd team for their logistical and technical support, particularly Melanie Leighton, Samantha Kemp, Lachlan Macdonald, Bruce Hunter, Cristian Vasquez, Antonio Muñoz Algobia, Ana Centeno, Pablo Torres and Andrea Aravena. Sharon Ness and Evgenia Lebedeva are thanked for their insights into QXRD analysis. This manuscript benefitted from the reviewers comments and insights, which included those of Dogan Paktunc.

References

ALS Geochemistry, 2018, Schedule of Services and Fees 2018 AUD (https://www.alsglobal.com/au/services-and-products/geochemistry/geochemistry-downloads)

Barton, M.D., 2014, Iron Oxide(-Cu-Au-REE-P-Ag-U-Co) Systems, Treatise on Geochemistry, Elsevier, v. 13, p. 515–541.

Berry, R., Hunt, J., and McKnight, S., 2011, Estimating mineralogy in bulk samples: AusIMM International Geometallurgy Conference, 1st, Brisbane, Australia, 2011, p. 153–156.

Berry, R., O'Conner, L., Hunt, J., and Bradshaw, D., 2013, Theme Four: Texture-based liberation and recovery modelling, GeM (AMIRA P843A) - Technical Report 11, 82p.

Berry, R., Hunt, J., Parbhakar-Fox, A., and Lottermoser, B., 2015, Prediction of acid rock drainage (ARD) from calculated mineralogy: International Conference on Acid Rock Drainage and IMWA Annual Conference, 10th, Santiago, 2015, p. 1–10.

Brown, M., Diáz, F., and Grocott, J., 1993, Displacement history of the Atacama fault system 25°00 S – 27° 0S, northern Chile: Geological Society of America Bulletin, v. 105, p. 1165–1174.

Bryan, W.B., Finger, L.W., and Chayes, F., 1969, Estimating proportions in petrographic mixing equations by least-squares approximation: Science, v. 163, p. 926–927.

Burnham, C. W., 1979, Magmas and hydrothermal fluids, in Barnes H.L., ed., Geochemistry of hydrothermal ore deposits, 3rd ed.: New York, Wiley, p. 71-136.

Clark A.H., and Arancibia, O.N., 1995, The occurrence, paragenesis and implications of magnetite-rich alteration-mineralization in calc-alkaline porphyry copper deposits: Giant Ore Deposits Workshop, 2nd, Kingston, Ontario, Canada, April 25-27, 1995, Proceedings, p. 511–581.

Cobeñas, G., and Halley, S., 2015, Using assay data to map mineralogy and alteration to help develop a predictive geometallurgical model for the Taca Taca Cu-Mo-Au porphyry deposit, Argentina: SEG 2015: World-Class Ore Deposits: Discovery to Recovery, Hobart, 2015.

Cox, K.G., Bell, J.D. and Pankhurst, R.J., 1979, The Interpretation of Igneous Rocks: Springer Netherlands, 450 p.

Cruz, N., Peng, Y., Farrokhpay, S., and Bradshaw, D., 2013, Interactions of clay minerals in copper–gold flotation: Part 1 – Rheological properties of clay mineral suspensions in the presence of flotation reagents: Minerals Engineering, v. 50–51, p. 30–37.

Dana, J.D., and Hurlbut, C.S., 1971, Dana's Manual of mineralogy: New York, Wiley, p. 609.

Davies, J,F., and Whitehead, R.E., 2006, Alkali-alumina and MgO-alumina molar ratios of altered and unaltered rhyolites: Exploration and Mining Geology, v. 15, p. 75-88.

Donskoi, E., Suthers, S.P., Campbell, J.J., and Raynlyn, T., 2008, Modelling and optimization of hydrocyclone for iron ore fines beneficiation — using optical image analysis and iron ore texture classification: International Journal of Mineral Processing, v. 87, p. 106–119.

Donskoi, E., Suthers, S.P., Fradd, S.B., Young, J.M., Campbell, J.J., Raynlyn, T.D., and Clout, J.M.F., 2007, Utilization of optical image analysis and automatic texture classification for iron ore particle characterisation: Minerals Engineering, v. 20, p. 461–471.

Escolme, A.J., 2016, Geology, geochemistry and geometallurgy of the Productora Cu-Au-Mo deposit, Chile: Unpublished PhD thesis, Hobart, Tasmania, University of Tasmania, 313 p.

Fandrich, R., Gu, Y., Burrows, D., and Moeller, K., 2007, Modern SEM-based mineral liberation analysis: International Journal of Mineral Processing, v. 84, p. 310–320.

Farrokhpay, S., and Bradshaw, D.J., 2012, Effect of clay minerals on froth stability in mineral flotation: a review: 26th International Mineral Processing Congress, IMPC 2012: Innovative Processing for Sustainable Growth-Conference Proceedings, New Delhi, India, 2012, p. 4601–4611.

Farrokhpay, S., and Ndlovu, B., 2013, Effect of phyllosilicate minerals on the rheology, colloidal and flotation behaviour of chalcopyrite mineral, Chemeca 2013: Australasian Conference on Chemical Engineering: Brisbane, QLD, Australia, Institution of Engineers, Australia, p. 1–7.

Forrest, M., 2009, Geometallurgy for mine data: Materials World, v. 17, p. 48–50.

Fox, K.A., 2000, Fe-Oxide (Cu-U-Au-REE) Mineralisation and Alteration at the Productora Prospect: Unpublished M.Sc. thesis, Golden, Colorado, Colorado School of Mines, 114 p.

Gu, Y., 2003, Automated scanning electron microscope based mineral liberation analysis: Journal of Minerals and Materials Characterization and Engineering, v. 2, p. 33–41.

Halley, S., Dilles, J. H., and Tosdal, R. M., 2015, Footprints: Hydrothermal alteration and geochemical dispersion around porphyry copper deposits: Society of Economic Geology Newsletter, v. 100, p. 12-17.

Halley, S., Wood, D., Stoltze, A., Godfroid, J., Goswell, H., and Jack, D., 2016, Using multielement geochemistry to map multiple components of a mineral system: Case study from a sediment-hosted Cu-Ni camp, NW Province, Zambia: Society of Economic Geologists Newsletter, v. 104, p. 15-21.

Helle, S., Kelm, U., Barrientos, A., Rivas, P., and Reghezza, A., 2005, Improvement of mineralogical and chemical characterization to predict the acid leaching of geometallurgical units from Mina Sur, Chuquicamata, Chile: Minerals Engineering, v. 18, p. 1334–1336.

Hemley, J.J., Cygan, G.L., Fein, J.B., Robinson, G.R., and D'Angelo, W.M., 1992, Hydrothermal ore-forming processes in the light of studies of rock-buffered systems: I. Iron–copper–zinc–lead sulfide solubility relations: Economic Geology, v. 87, p. 1–22.

Hoal, K.O., 2008, Getting the geo into geomet: SEG Newsletter, Society of Economic Geologists, v. 73, p. 11–15.

Hoal, K.O., Appleby, S. K., Stammer, J.G., and Palmer, C., 2009, SEM-based quantitative mineralogical analysis of peridotite, kimberlite, and concentrate: Lithos, v. 112, Supplement 1, p. 41–46.

Hot Chili Ltd, 2016, ASX announcement: Wednesday 2nd March 2016, Hot Chili delivers PFS and near doubles reserves at Productora (http://www.hotchili.net.au/assets/Uploads/HCH5Productora-Delivers-PFS-Resource-Reserve-Upgrade02032016.pdf)

Hunt, J., Berry, R., Walters, S., Bonnici, N., Kamenetsky, M., Nguyen, K., and Evans, C., 2008, A new look at mineral maps and the potential relationships of extracted data to mineral processing behaviours: Australasian Institute of Mining and Metallurgy Publication Series, 2008, p. 429–432.

Knorr, K., 2010, Advances in quantitative x-ray mineralogy: Process Mineralogy, v. 10, p. 10–12.

Lamberg, P., 2011, Particles–the bridge between geology and metallurgy: Proceedings of the Conference in Minerals Engineering, Luleå, Sweden, 2011, p. 8–9.

Lane, G.R., Martin, C., and Pirard, E., 2008, Techniques and applications for predictive metallurgy and ore characterization using optical image analysis: Minerals Engineering, v. 21, p. 568–577.

Lawson, C.L., and Hanson, R.J., 1995, Solving Least Squares Problems: Philadelphia, SIAM, 337 p.

Le Maitre, R.W., 1981, GENMIX - a generalized petrological mixing model program: Computers & Geosciences, v. 7, p. 229–247.

Le Maitre, R.W., 1989, A classification of igneous rocks and glossary of terms: Recommendations of the International Union of Geological Sciences Subcommission on the Systematics of Igneous Rocks: Oxford, Blackwell, 193 p.

Liipo, J., Lamberg, P., Turunen, J., and Pitkäjärvi, J., 2004, Grain Size and Liberation of Chromite in Ground Chrome Ore from Kemi Mine, Finland, ICAM 2004 - The 8th International Congress on Applied Mineralogy: Developments in Science and Technology: Aquas de Lindoia, Brazil, p. 1005-1007.

Luhr, J.F., and Carmichael, I.S.E., 1980, The Colima volcanic complex, Mexico. I: post-caldera andesites from Volcan Colima: Contributions to Mineralogy and Petrology, v. 71, p. 343-372.

Lund, C., and Martinsson, O., 2008, A characterising of the ore minerals due to mineralogical, chemical and textural properties in Malmberget: Conference in Minerals Engineering, 2008, p. 71–80.

Lund, C., Martinsson, O., and Lindberg, T., 2010, Mineralogical-textural characterisation of different apatite-iron ore bodies, Malmberget deposit, Sweden, treated in a sorting process in laboratory scale, Process Mineralogy'10: Cape Town, South Africa, p. 208-216.

Ménard, J.J., 1995, Relationship between altered pyroxene diorite and the magnetite mineralization in the Chilean Iron Belt, with emphasis on the El Algarrobo iron deposits (Atacama region, Chile): Mineralium Deposita, v. 30, p. 268–274.

Montoya, P., Keeney, L., Jahoda, R., Hunt, J., Berry, R., Drews, U., Chamberlain, V., and Leichliter, S., 2011, Geometallurgical modelling techniques applicable to prefeasability projects-La Colosa case study: Geomet 2011 -The First AusIMM International Geometallurgical Conferenece, Brisbane, Australia, 2011, p. 103–112.

Omotoso, O., McCarty, D.K., Hillier, S., and Kleeberg, R., 2006, Some successful approaches to quantitative mineral analysis as revealed by the 3rd Reynolds Cup contest: Clays and Clay Minerals, v. 54, p. 748–760.

Oghazi, P., Pålsson, B., and Tano, K., 2009, Applying traceability to grinding circuits by using particle texture analysis (PTA): Minerals Engineering, v. 22, p. 710–718.

Paktunc, A.D., 1998, MODAN: an interactive computer program for estimating mineral quantities based on bulk composition: Computers & Geosciences, v. 24, p. 425–431.

Paktunc, A.D., 2001, MODAN—a computer program for estimating mineral quantities based on bulk composition: windows version: Computers and Geosciences, v. 27, p. 883-886.

Parbhakar-Fox, A., and Lottermoser, B.G., 2015, A critical review of acid rock drainage prediction methods and practices: Minerals Engineering, v. 82, p. 107-124.

Petruk, W., 1989, Short Course on Image Analysis Applied to Mineral and Earth Sciences, in Pertuk, W., ed., Mineralogical Association of Canada Short Course, v. 16, p. 6–18.

Pignolet-Brandom, S., and Reid, K.J., 1988, Mineralogical Characterization by QEM*SEM, in Carson, D.J.T., Vassoilou, A.H., and Warrendale, T.M.S, eds., Process Mineralogy VIII, p. 337–346.

Press, W.H., Flannery, B.P., Teukolsky, S.A., and Vetterling, W.T., 1986, Numerical Recipes: The art of scientific computing, Cambridge, Cambridge University Press, 818 p.

Whitney, J.A., Hemley, J.J., and Simon, F.O., 1985, The concentration of iron in chloride solutions equilibrated with synthetic granite compositions: The sulfur-free system: Economic Geology, v. 80, p. 444–460.

Table Captions

TABLE 1. Absolute error estimates for QXRD analysis (S. Ness, pers. commun., 2014). Note, absolute error is the magnitude of the difference between exact value and approximation.

TABLE 2. Summary of model performance parameters for major minerals and mineral groups calculated by linear programming compared to QXRD measured values corrected against chemical assays by weighted least squares (WLSQ). Listed in order of decreasing R^2.

TABLE 3. Parameters used for modelling calculated mineralogy data in 3D as interpolants.

Figure Captions

FIG 1. Steps of a geometallurgical program, modified from Lamberg (2011).

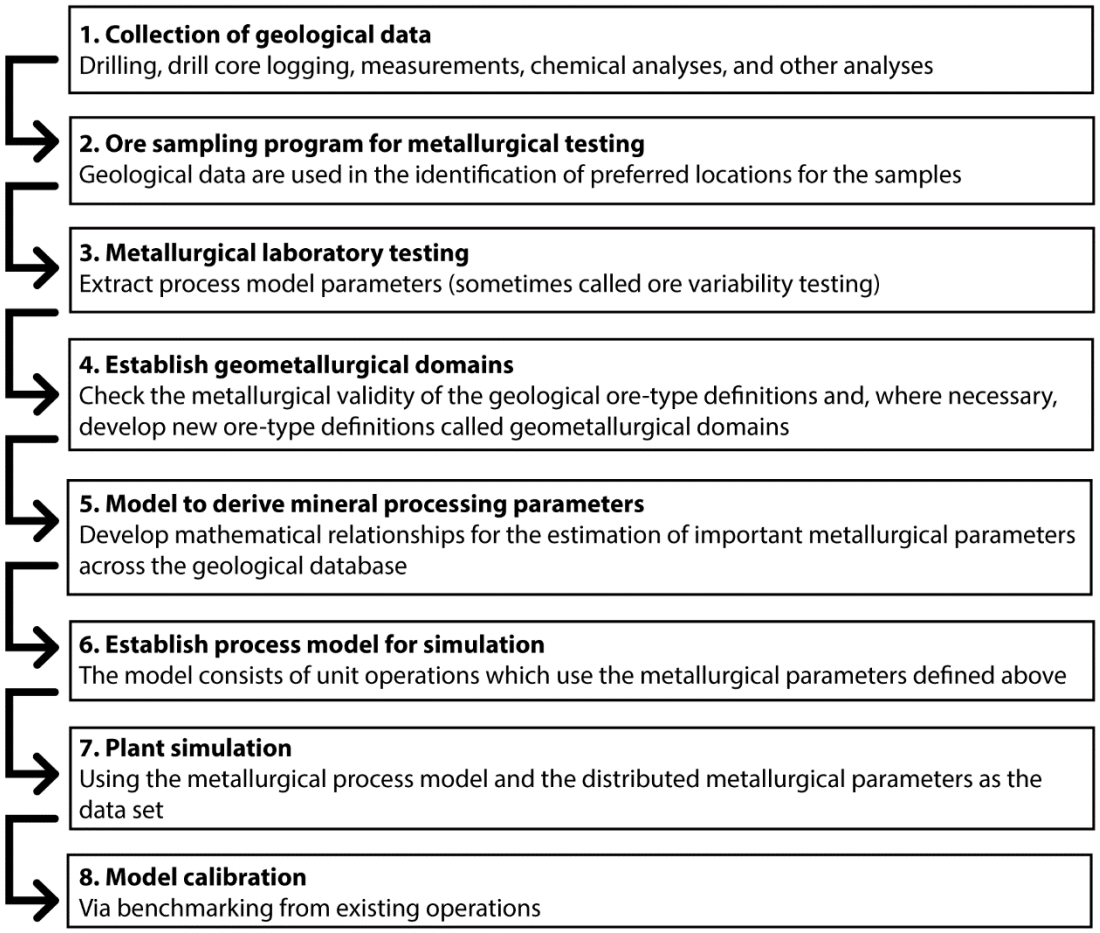

FIG 2. Location and geology of the Productora Cu-Au-Mo deposit, Chile (redrawn from Escolme, 2016). A) Location map showing Atacama Fault System from Brown et al. (1993). B) Map showing local geology and major structures from surface mapping. Also shown is a surface projection of the mineralization limits (defined as >0.1 %Cu projected to surface) and location of study sections at 6,822,215 mN and 6,820,850 mN. Modified from Ray and Dick (2002), Beeson (2012) and J. Beeson pers. comm. (2015). Cross sections at C) 6,822,215 mN and D) 6,820,850 mN showing geology interpreted from graphic core logging, core photo logging and immobile element lithogeochemistry. Breccia domains reflect variations in texture and internal clast organization — protolith textures were largely obscured by alteration and brecciation in these domains. Whilst several phases of basalt-andesite and dacite dykes are present, for clarity these are not shown.

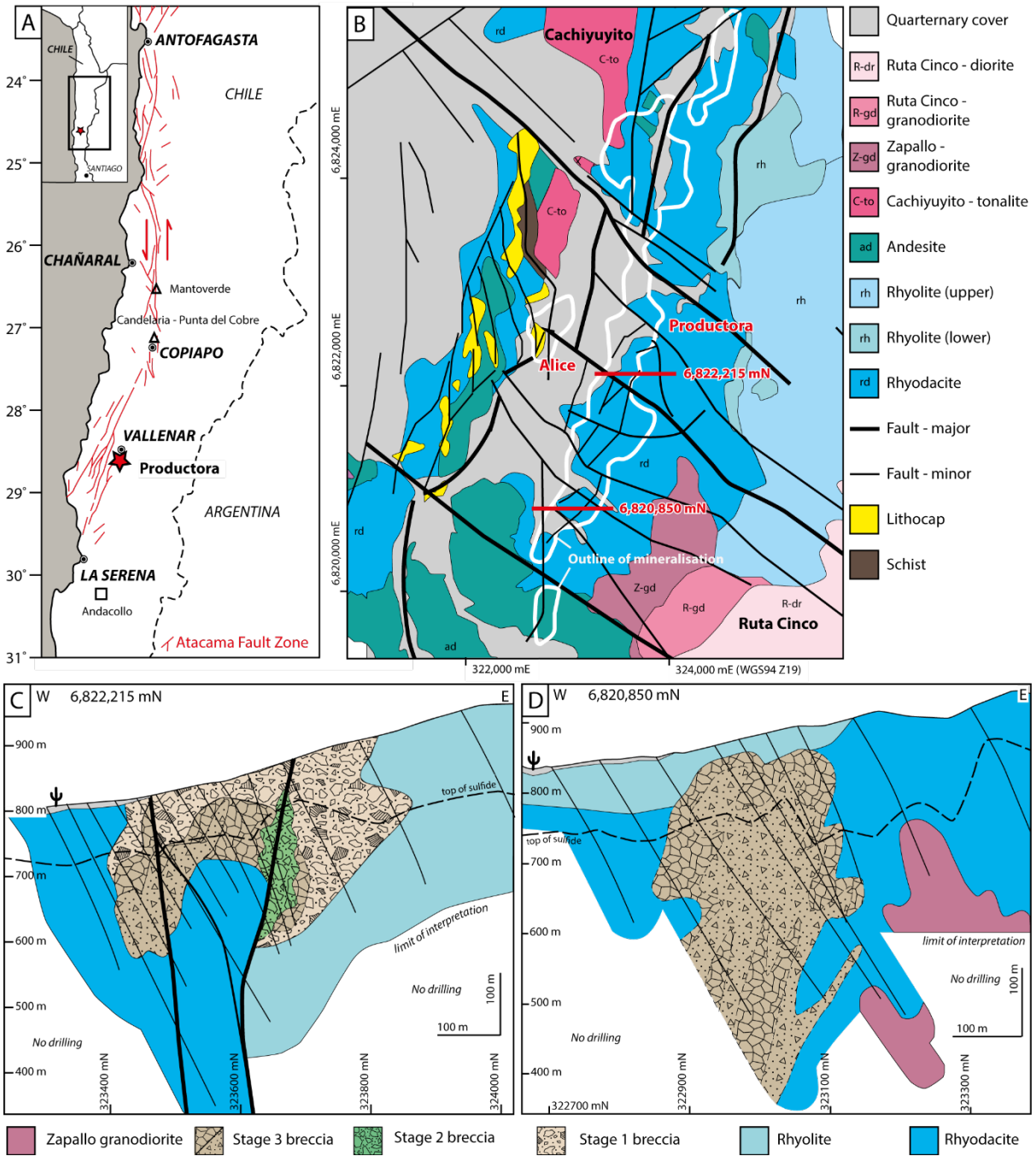

FIG 3. Results of weighted least squares correction of QXRD data (WLSQ) plotted against raw QXRD data for twelve of the 36 minerals calculated. Best fit regression lines and R^2 also shown. A) Quartz. B) K-feldspar. C) Muscovite (including illite). D) Plagioclase (including sodic and calcic plagioclase). E) Kaolinite. F) Epidote. G) Fe-oxides (magnetite, hematite and goethite). H) Chalcopyrite. I) Calcite. J) Anhydrite and gypsum. K) Apatite. L) Molybdenite. Minerals with low abundance, such as molybdenite and apatite, are poorly represented by the raw QXRD data which has relatively high detection limit (0.5 wt %), but are well constrained by the assay data hence the relationship between WLSQ and QXRD is poor.

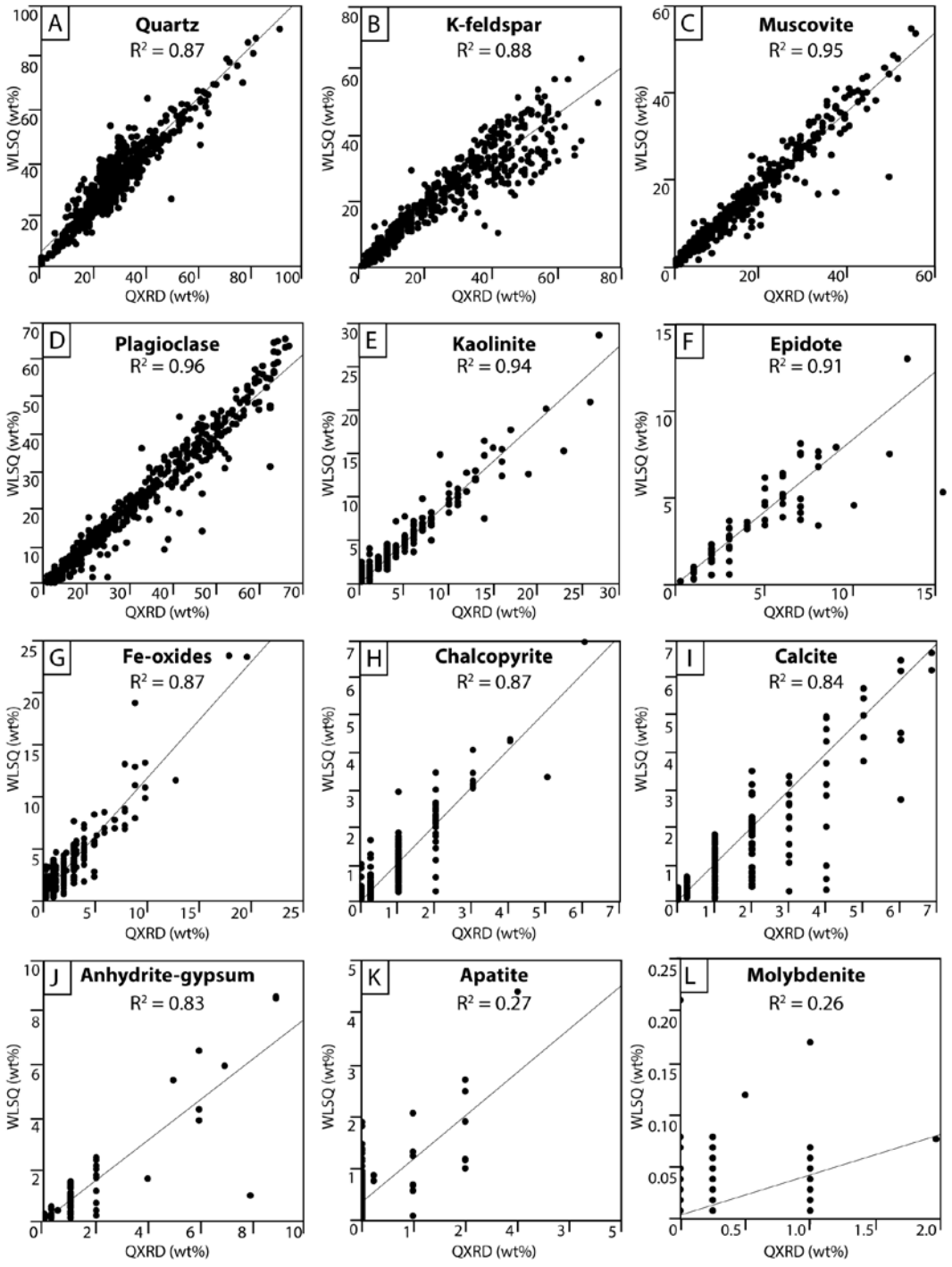

FIG 4. Tukey box plots showing wt % minerals estimated by weighted least squares calculation (WLSQ). Note the different scales for each diagram. Data colour coded by the cross section (red = 6,822,215 mN, blue = 6,820,850 mN). Mean = black dot, median = black horizontal line.

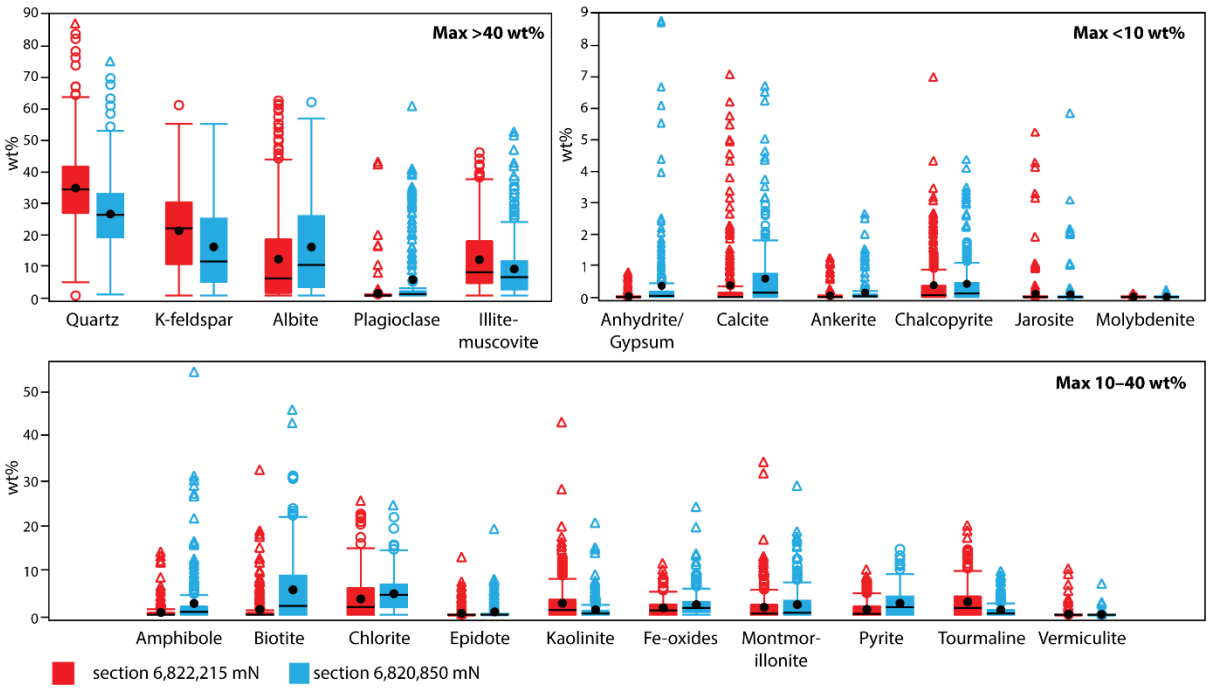

FIG 5. Workflow for classification of samples by dominant alteration type from whole rock geochemistry, based on case study dataset from Productora Cu-Au-Mo deposit, Chile.

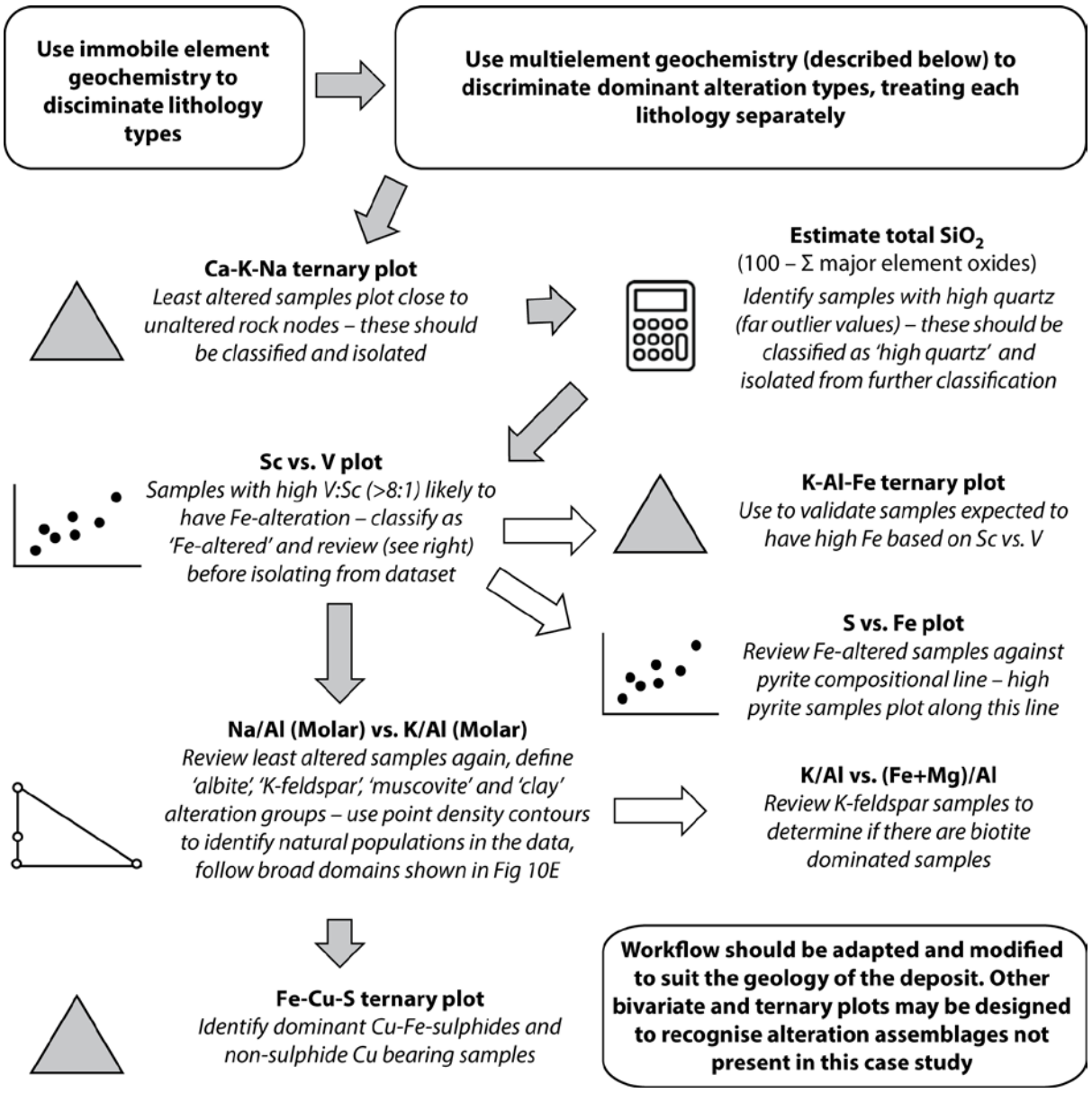

FIG 6. Productora training set plotted on a Ca-K-Na ternary diagram with nodes for unaltered igneous rocks from Cox et al., 1979. Samples plotting close to the unaltered host rock composition are classified as ‘least altered’.

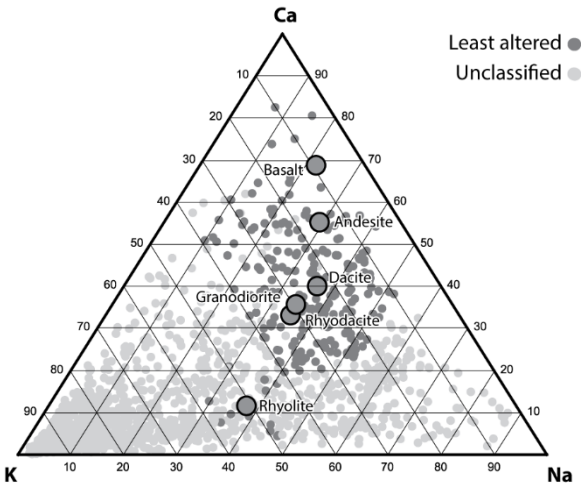

FIG 7. Comparison of A) SiO_2 calculated from geochemistry against SiO_2 calculated from WLSQ mineralogy. The strong correlation indicates that the calculation method from multielement geochemistry outlined in the text is robust. Comparison of SiO_2 calculated from geochemistry against WLSQ estimates of B) quartz, C) muscovite, D) total clays, E) K-feldspar, and F) as a tukey plot (mean = black dot, median = black horizontal line).

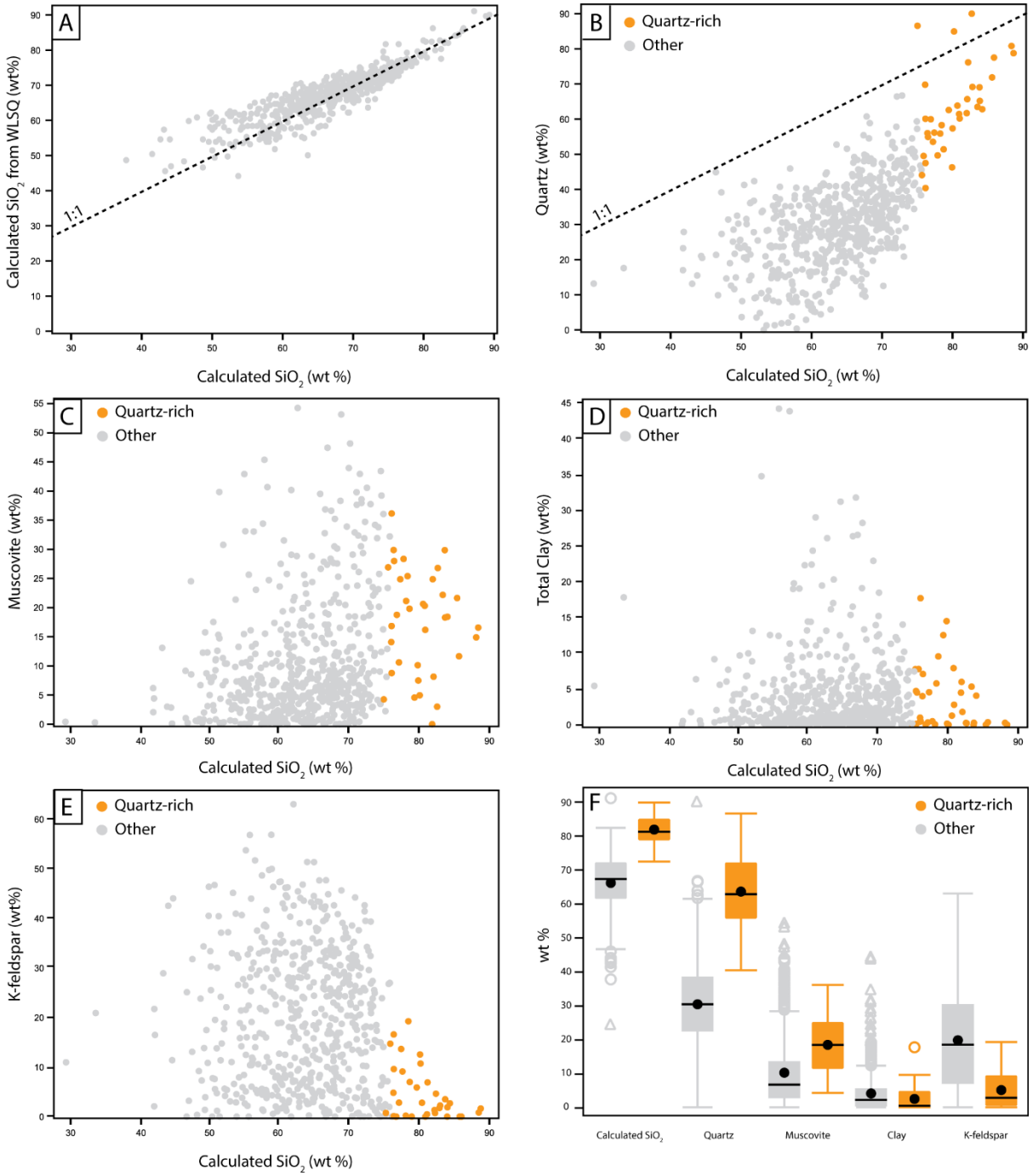

FIG 8. A) Plot of V against Sc to show discrimination of samples with high V:Sc ratio. B) Ternary plot of Al-K-Fe showing samples with high V/Sc value also show higher Fe/Al and Fe/K. C) Plot of V against Sc to show samples with high V/Sc also contain high Fe-oxides. D) Plot of Fe against S to show that most high Fe samples do not fall on the pyrite compositional tie line.

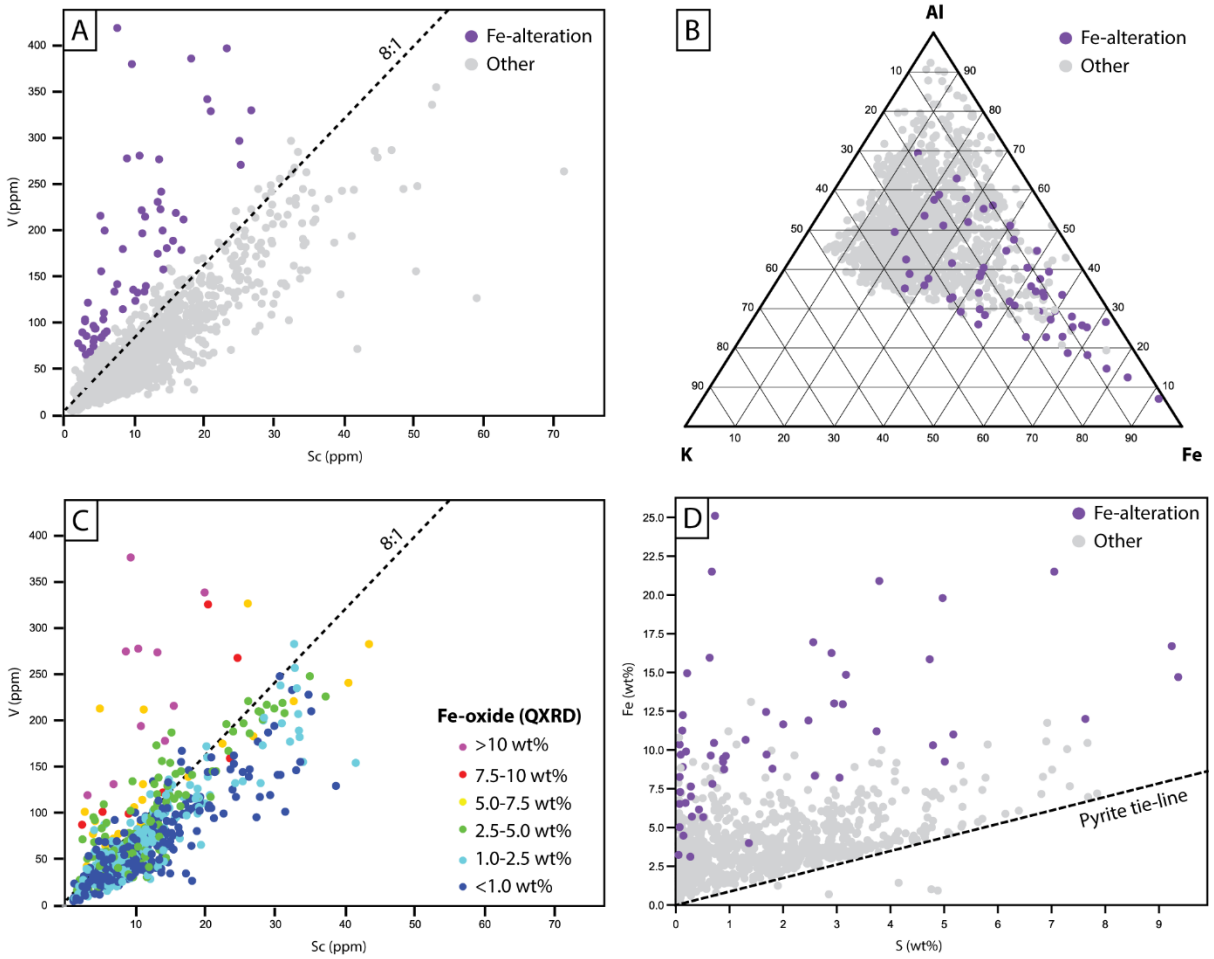

FIG 9. Tukey plot showing abundance of Fe-oxide, amphibole group minerals and apatite, estimated by WLSQ in each alteration classification group for 625 samples from two cross sections. Mean = black dot, median = black horizontal line.

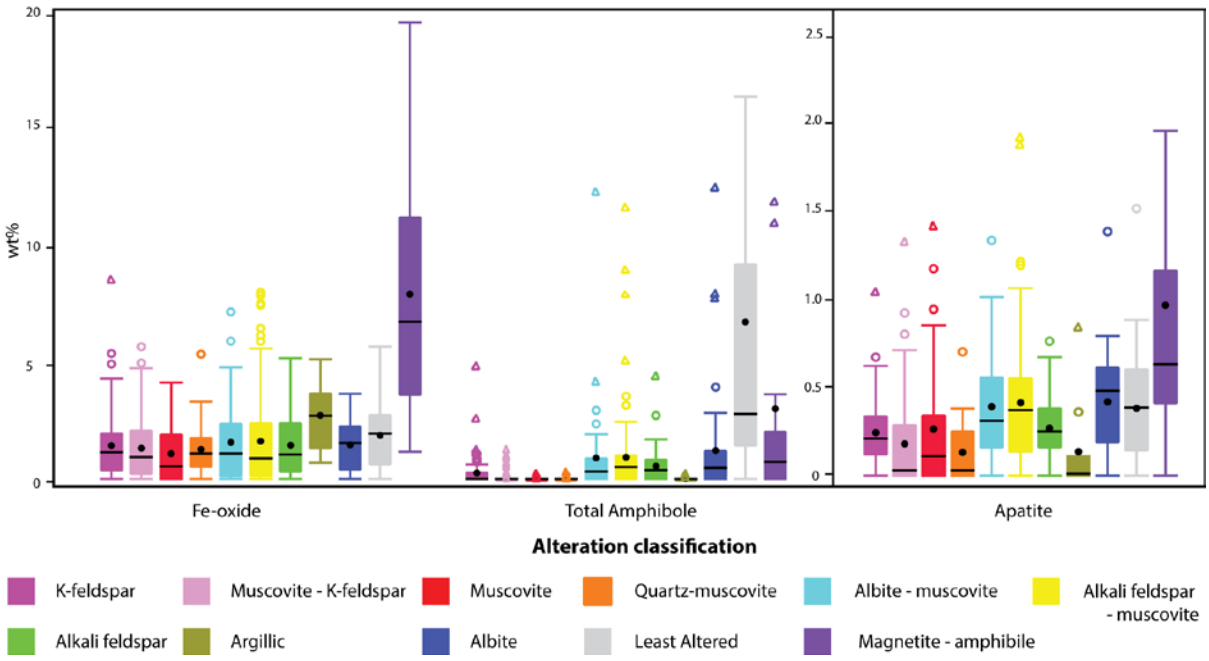

FIG 10. Alkali- (Na, K) alumina molar ratio plots, after Davies and Whitehead (2006), showing abundance of A) K-feldspar, B) albite, C) muscovite, and D) data density and E) user classification of data points by dominant mineralogy based on their position on the diagram. Mineral composition nodes based on stoichiometry, rock composition nodes from Cox et al., (1979). Ab = albite, Bt = biotite, Chl = chlorite, Ill = illite, Kfs = K-feldspar, Kln = kaolinite, Ms = muscovite, Olg = oligoclase, Phg = phengite.

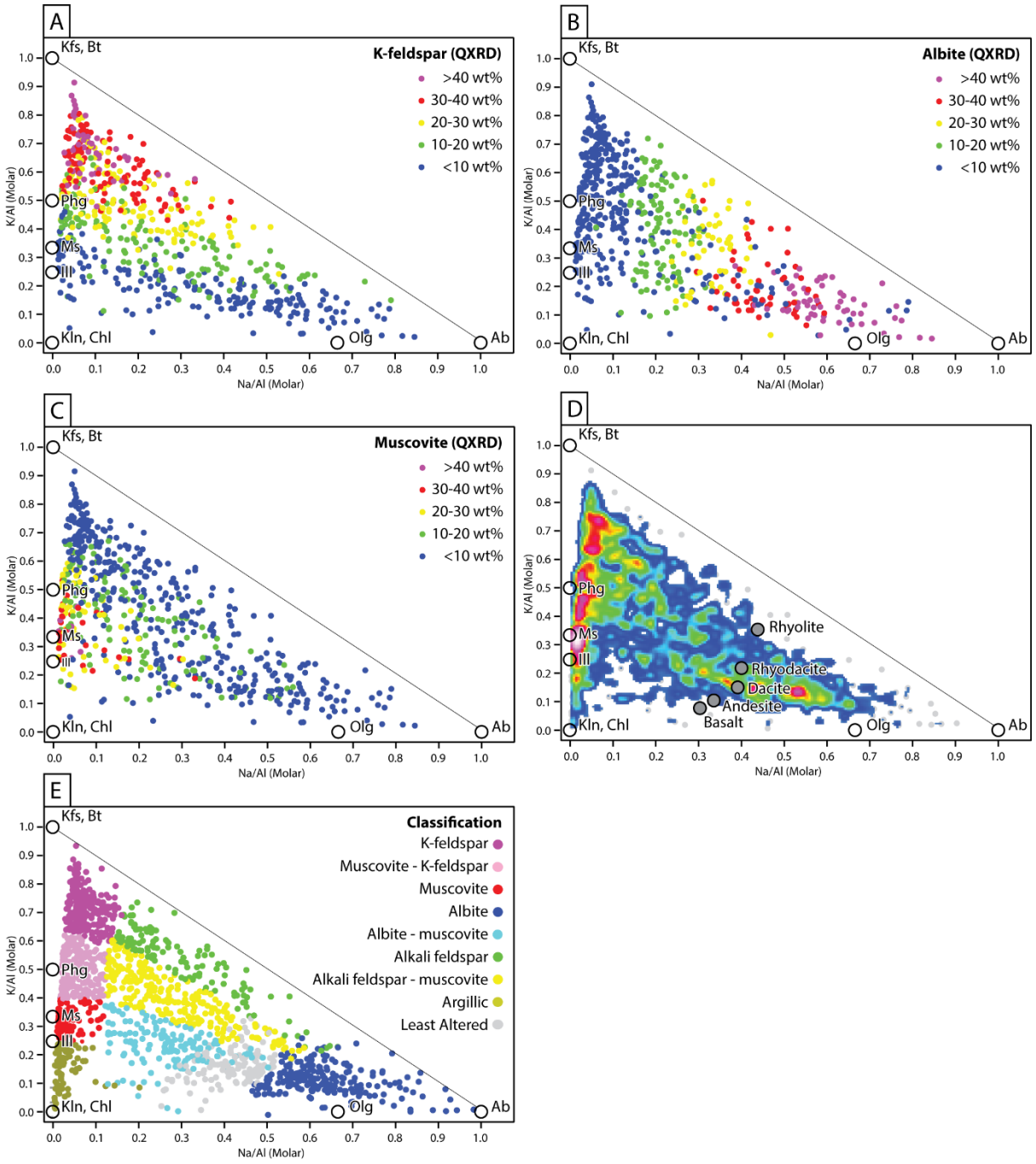

FIG 11. Tukey plot showing abundance of K-feldspar, muscovite, albite, quartz and kaolinite, measured by QXRD and corrected against assay data by weighted least squares calculation, in each alteration classification group for 625 samples from two cross sections. Mean = black dot, median = black horizontal line.

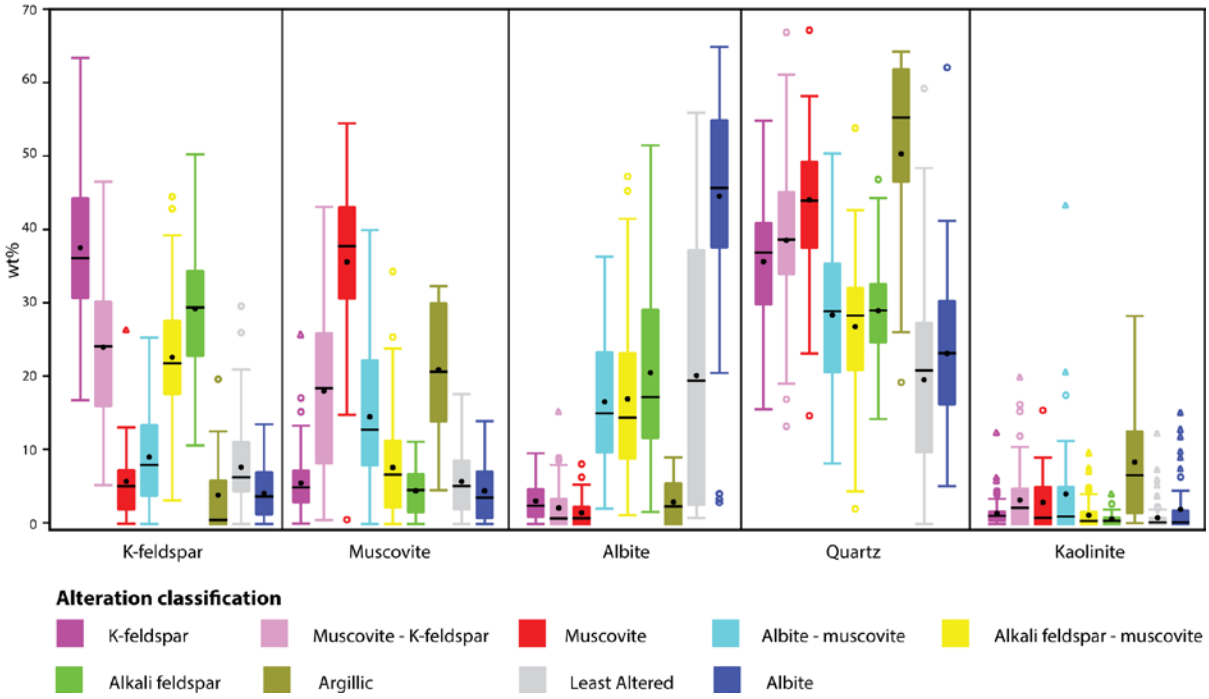

FIG 12. Ternary plots of Cu-Fe-S showing proportion of A) pyrite, B) chalcopyrite, C) chalcocite, D) non-sulfide Cu, and E) data density and F) classification of data points by dominant sulfide mineralogy. Mineral composition nodes based on stoichiometry. Barren samples classified as low Cu/S (<0.06) and low Fe/S (<0.04).

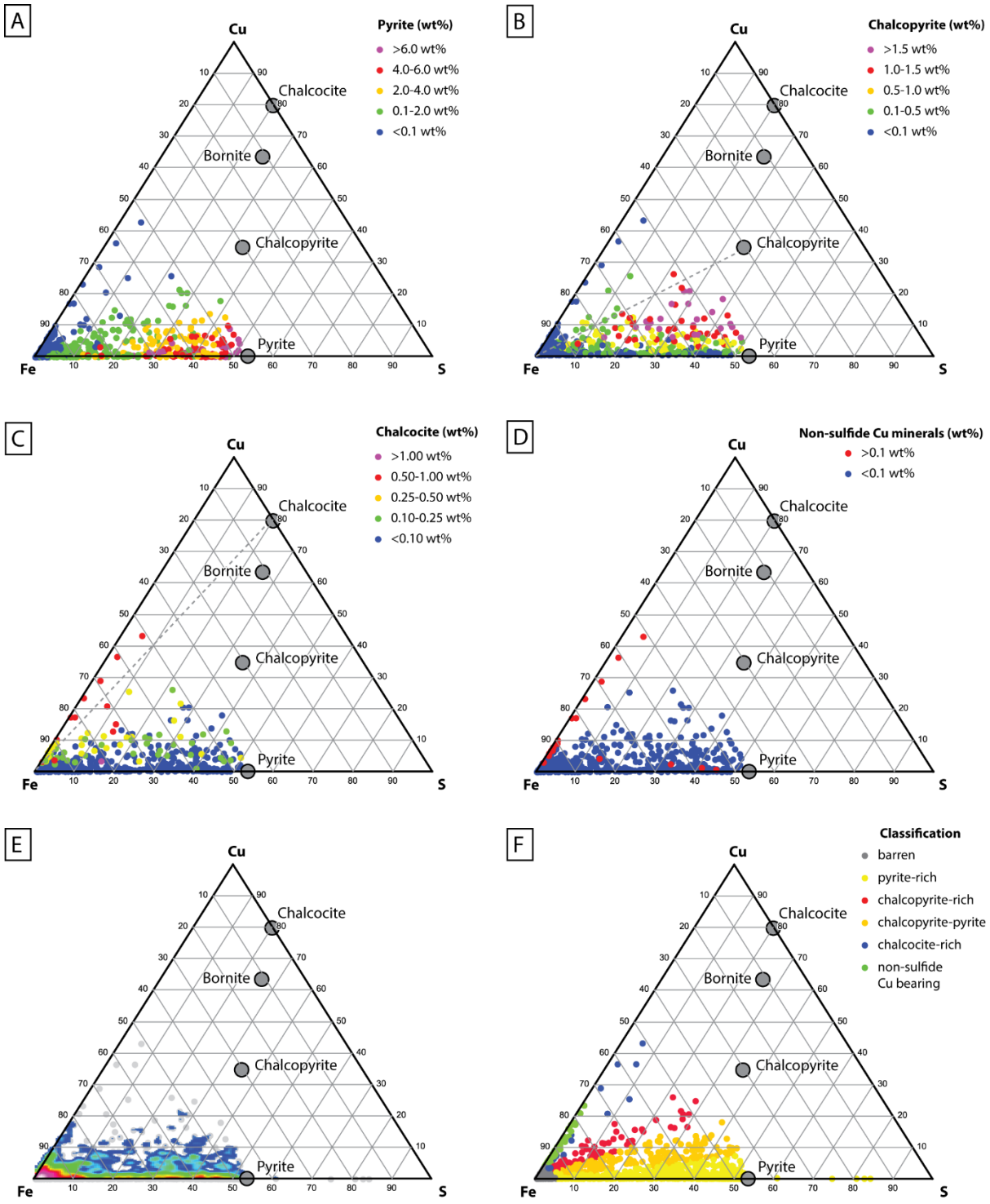

FIG 13. Tukey plot showing abundance of chalcocite, chalcopyrite, non-sulfide Cu and pyrite, as measured by QXRD and corrected against assay data by weighted least squares calculation, in each sulfide classification group for 625 samples from two cross sections. Mean = black dot, median = black horizontal line.

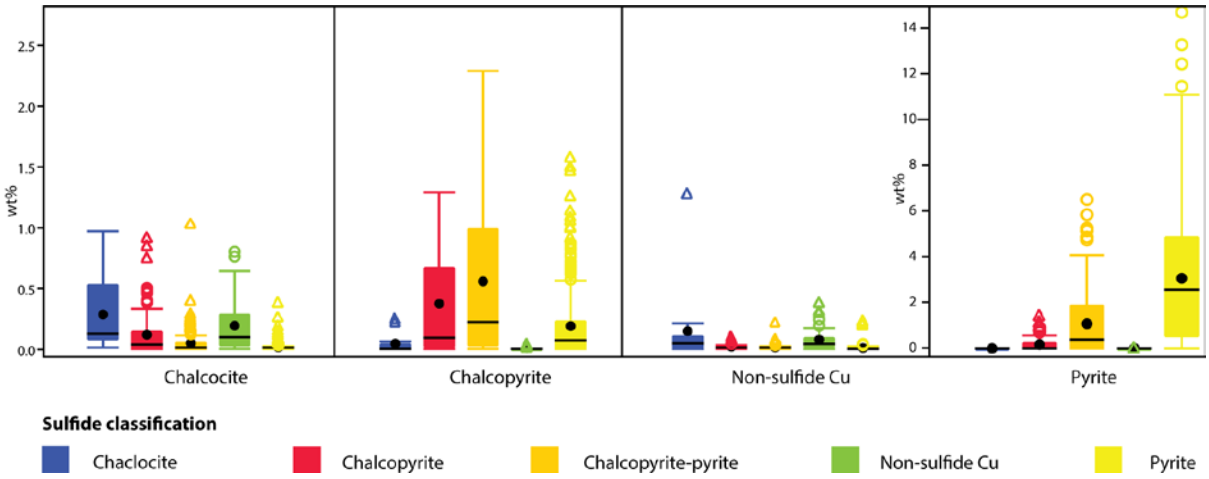

FIG 14. Cross section at 6,822,215 mN showing multielement assay samples (colored points along drillhole) classified by alteration geochemistry and interpreted domains of dominant alteration mineralogy (background color).

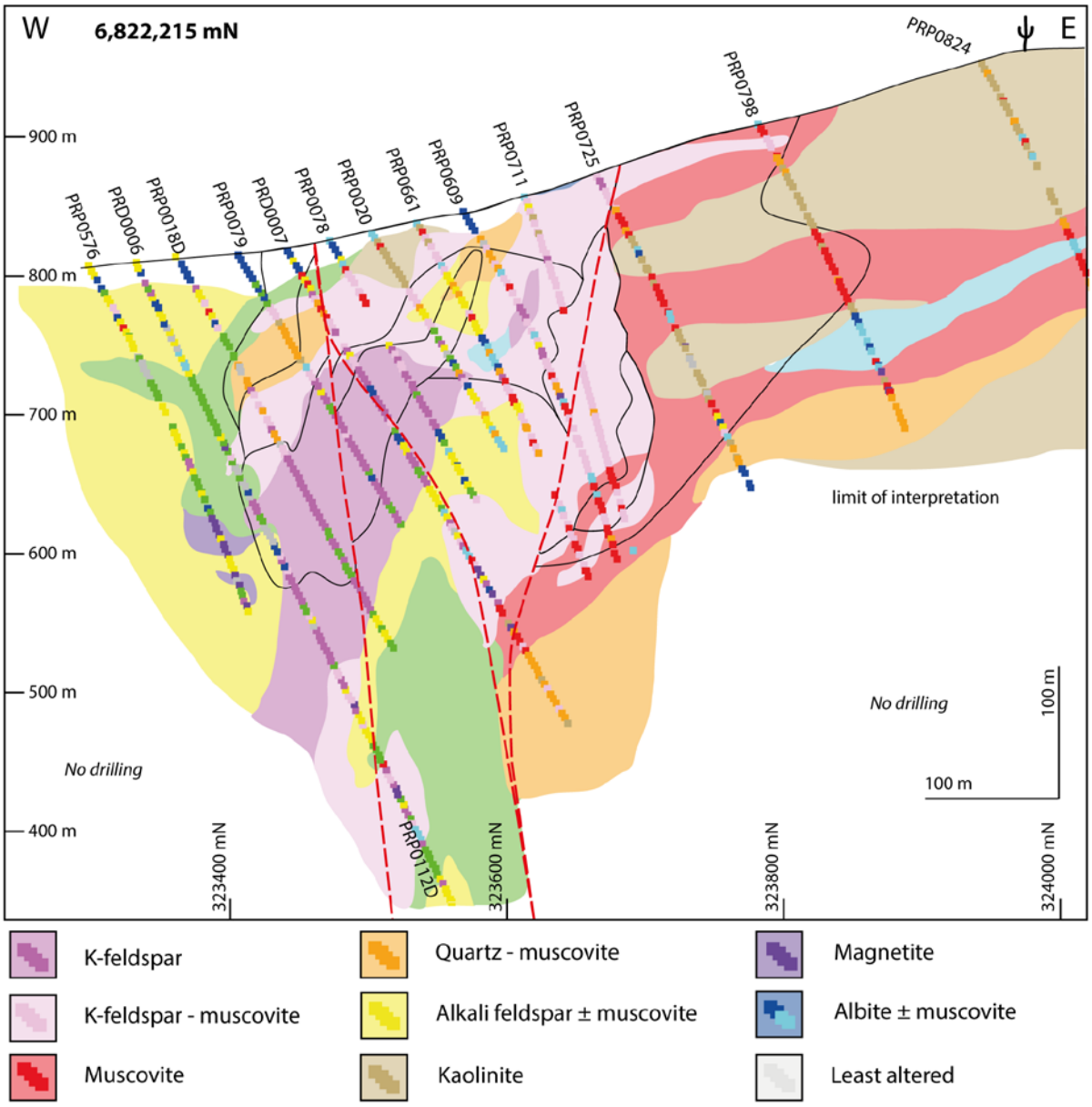

FIG 15. Cross section at 6,820,850 mN showing multielement assay samples (colored points along drillhole) classified by alteration geochemistry and interpreted domains of dominant alteration mineralogy (background color).

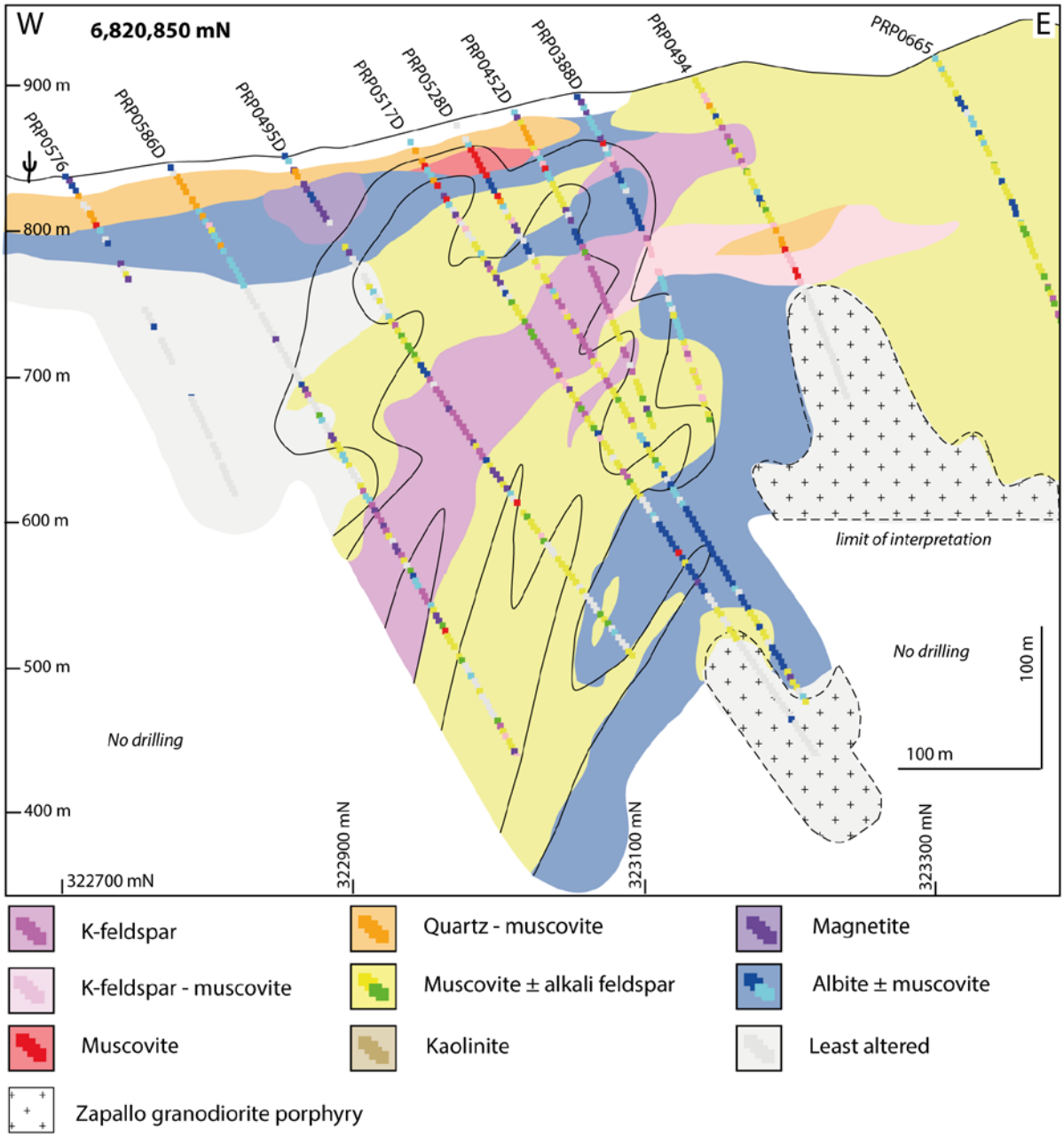

FIG 16. Cross section at 6,822,215 mN showing multielement assay samples (colored points along drillhole) classified by dominant sulfide based on geochemistry, and interpreted domains of dominant sulfide mineralogy (background color).

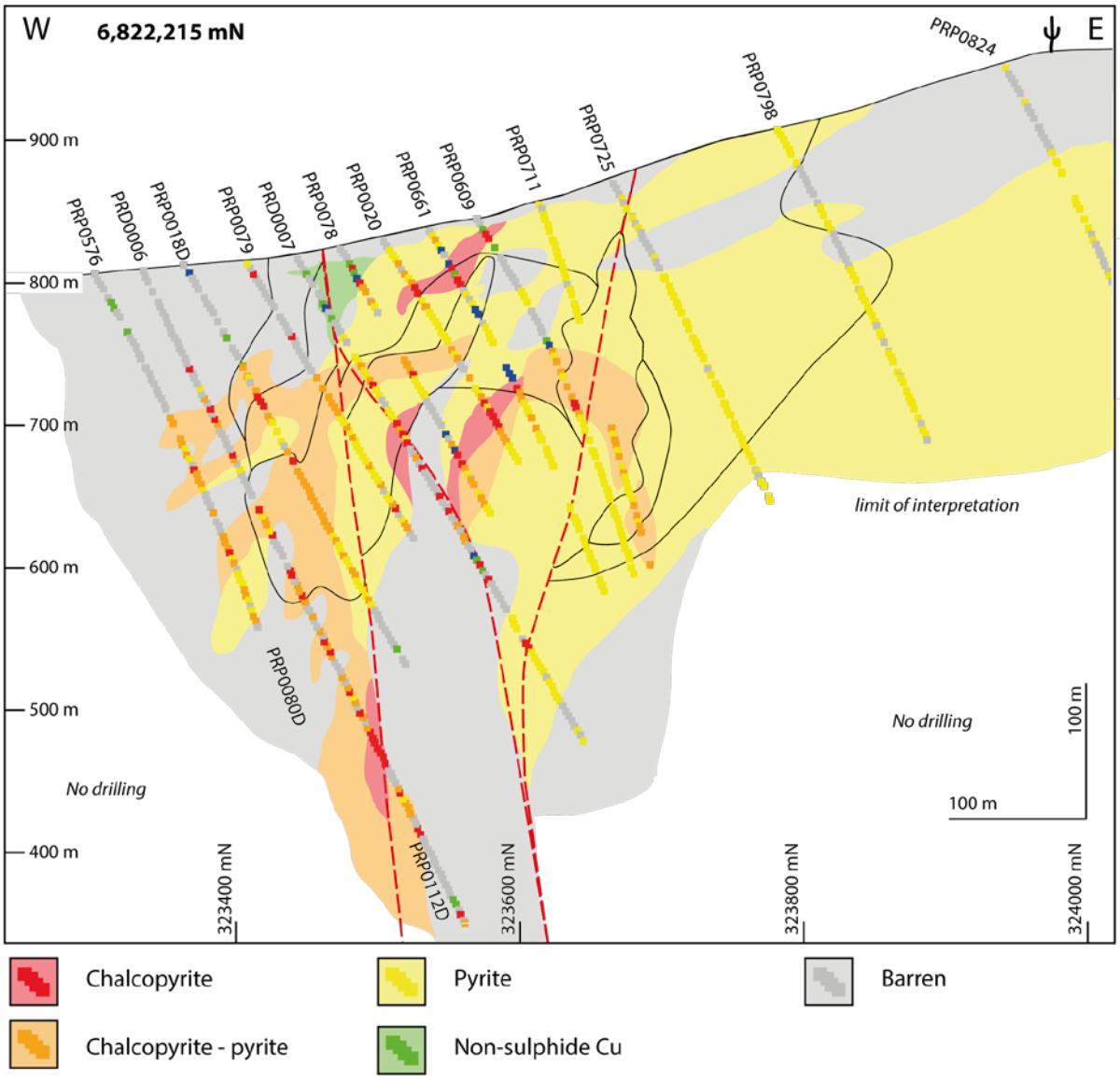

FIG 17. Cross section at 6,820,850 mN showing multielement assay samples (colored points along drillhole) classified by dominant sulfide based on geochemistry, and interpreted domains of dominant sulfide mineralogy (background color).

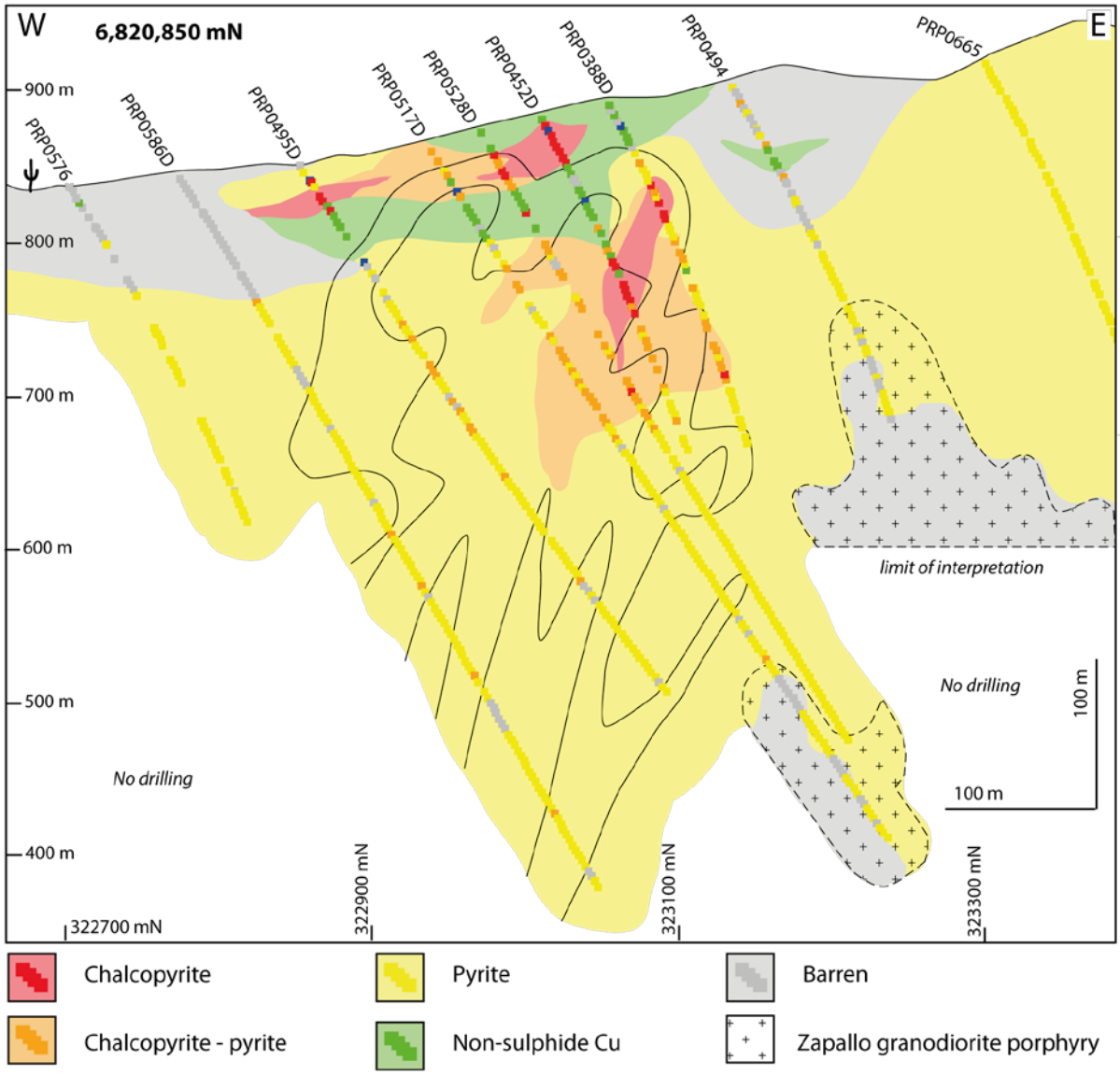

FIG 18. Comparison of WLSQ estimates against calculated mineralogy by linear programming. Regression line and R^2 also shown. A) Quartz. B) K-feldspar. C) Plagioclase (including sodic and calcic plagioclase). D) Pyrite. E) Chalcopyrite. F) Molybdenite. G) Total chlorite and micas (including chlorite, muscovite, phengite and biotites). H) Total clay (including kaolinite and smectite-montmorillonite). I) Fe-oxides (including magnetite, hematite, goethite). Major minerals, including quartz, feldspars, pyrite and Fe-oxides show excellent correlation between measured (WLSQ) and calculated (linear programming).

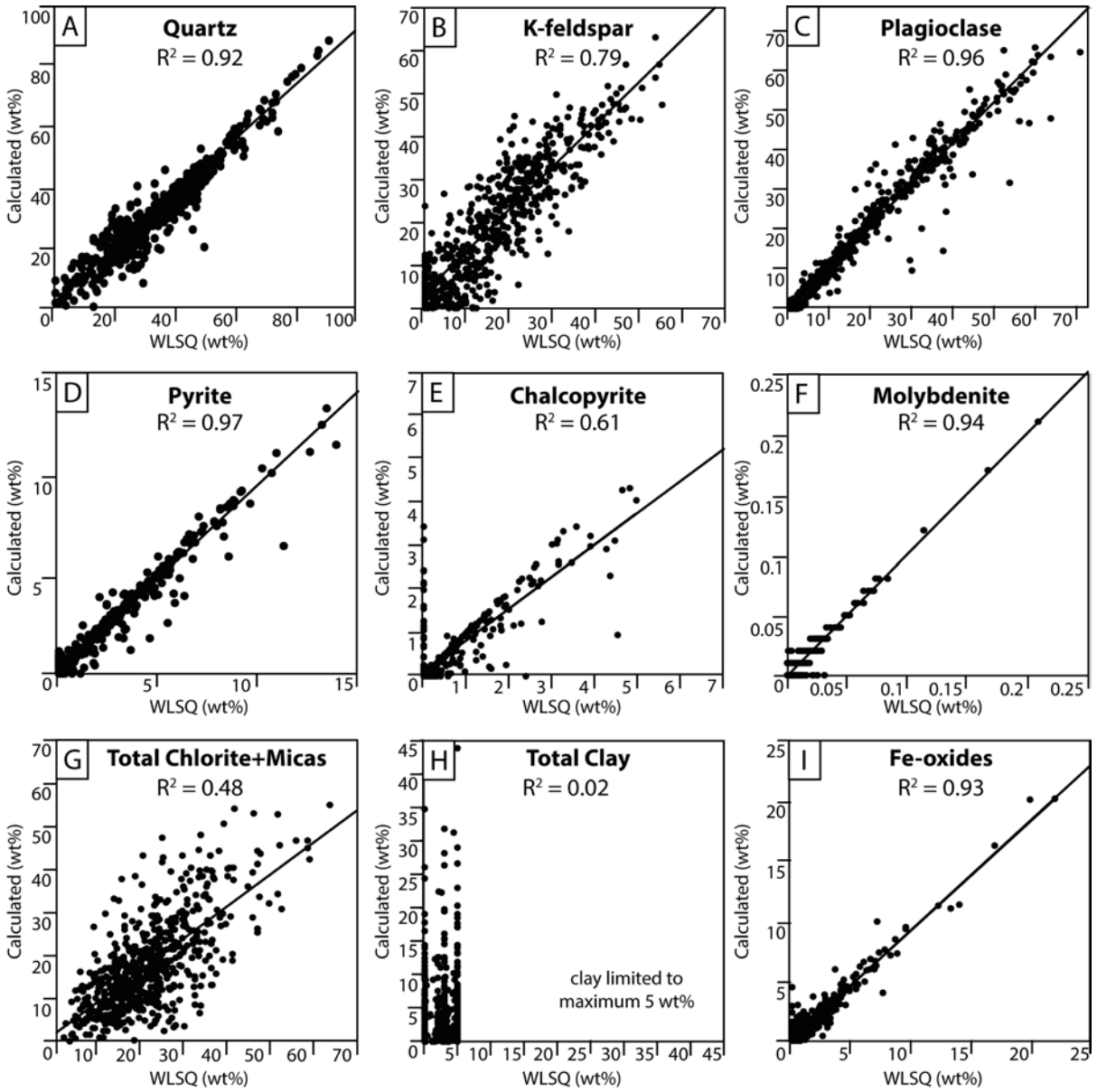

FIG 19. Section 6,822,215 mN comparison of calculated mineralogy by linear programming (LP) against WLSQ. Interpolants based only on LP data with equivalent WLSQ. A) LP total quartz and feldspar. B) WLSQ total quartz and feldspar. C) LP total chlorite and micas. D) WLSQ total chlorite and micas.

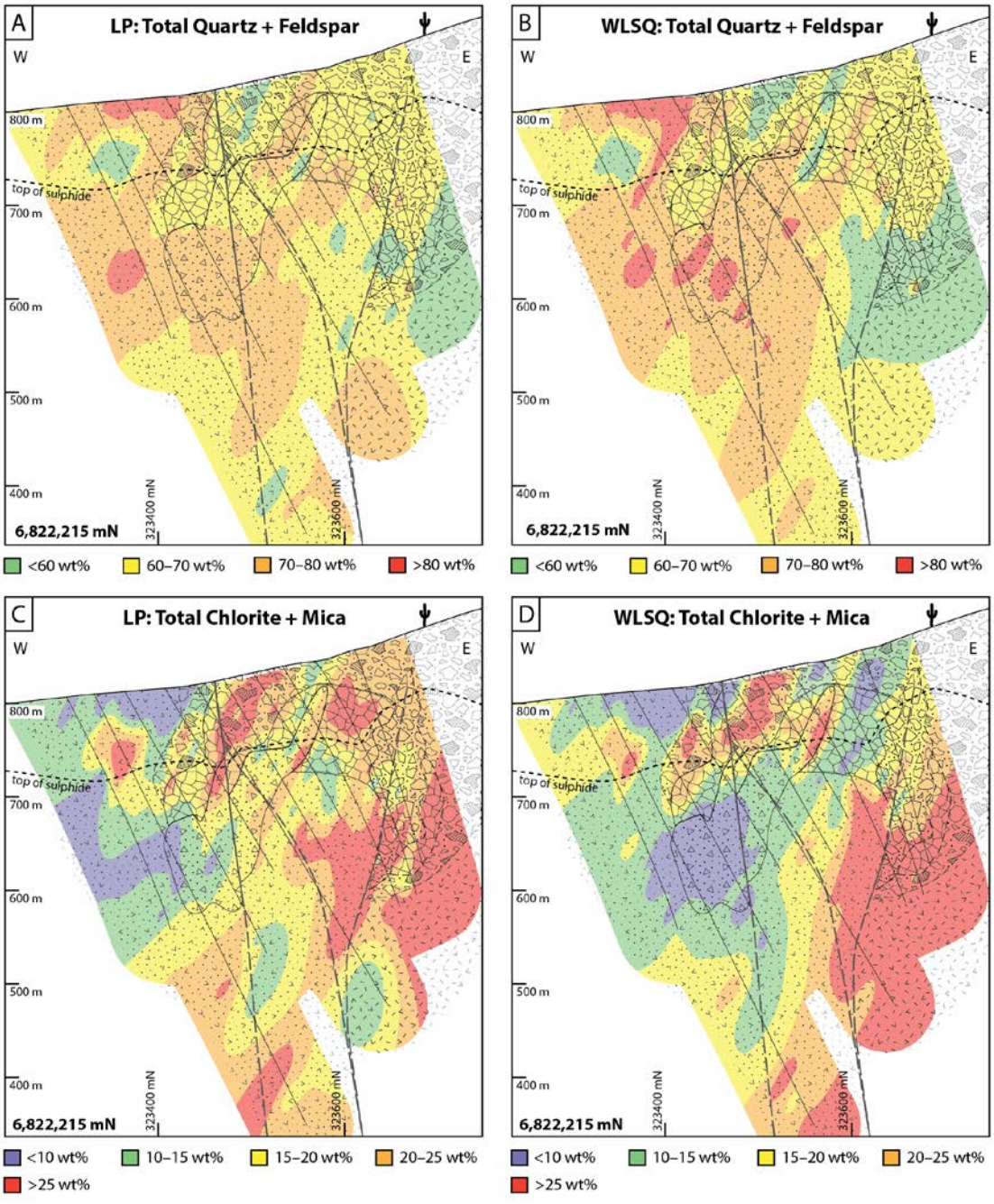

FIG 20. Section 6,822,215 mN comparison of calculated mineralogy by linear programming (LP) against WLSQ estimate. Interpolants based only on LP data with equivalent WLSQ. A) LP pyrite. B) WLSQ pyrite. C) LP total clay. D) WLSQ total clay.

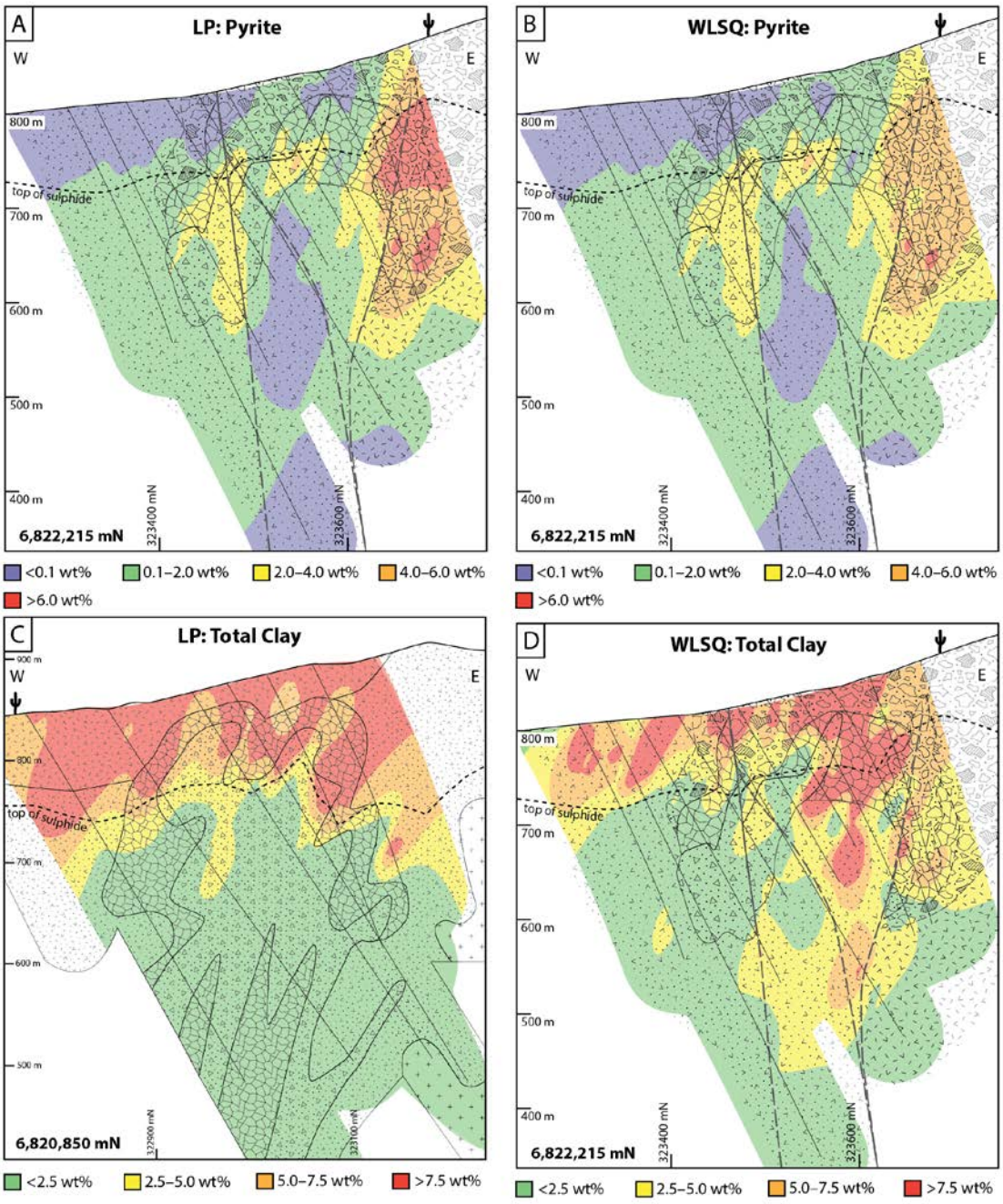

FIG 21. Section 6,820,850 mN comparison of calculated mineralogy by linear programming (LP) against WLSQ. Interpolants based only on LP data with equivalent WLSQ. A) LP total quartz and feldspar. B) WLSQ total quartz and feldspar. C) LP total chlorite and micas. D) WLSQ total chlorite and micas.

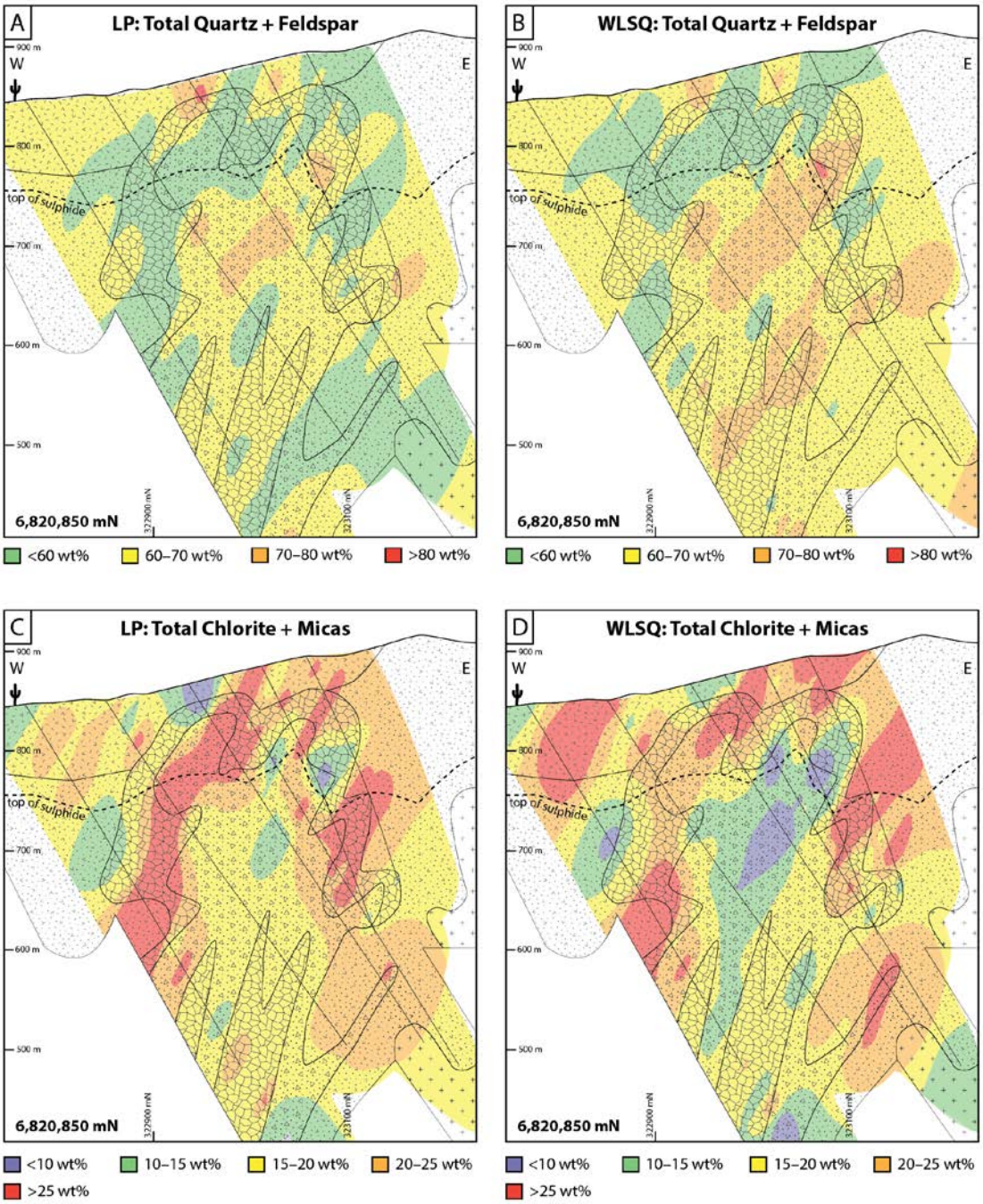

FIG 22. Section 6,820,850 mN comparison of calculated mineralogy by linear programming (LP) against WLSQ. Interpolants based only on LP data with equivalent WLSQ. A) LP pyrite. B) WLSQ pyrite. C) LP total clay. D) WLSQ total clay.

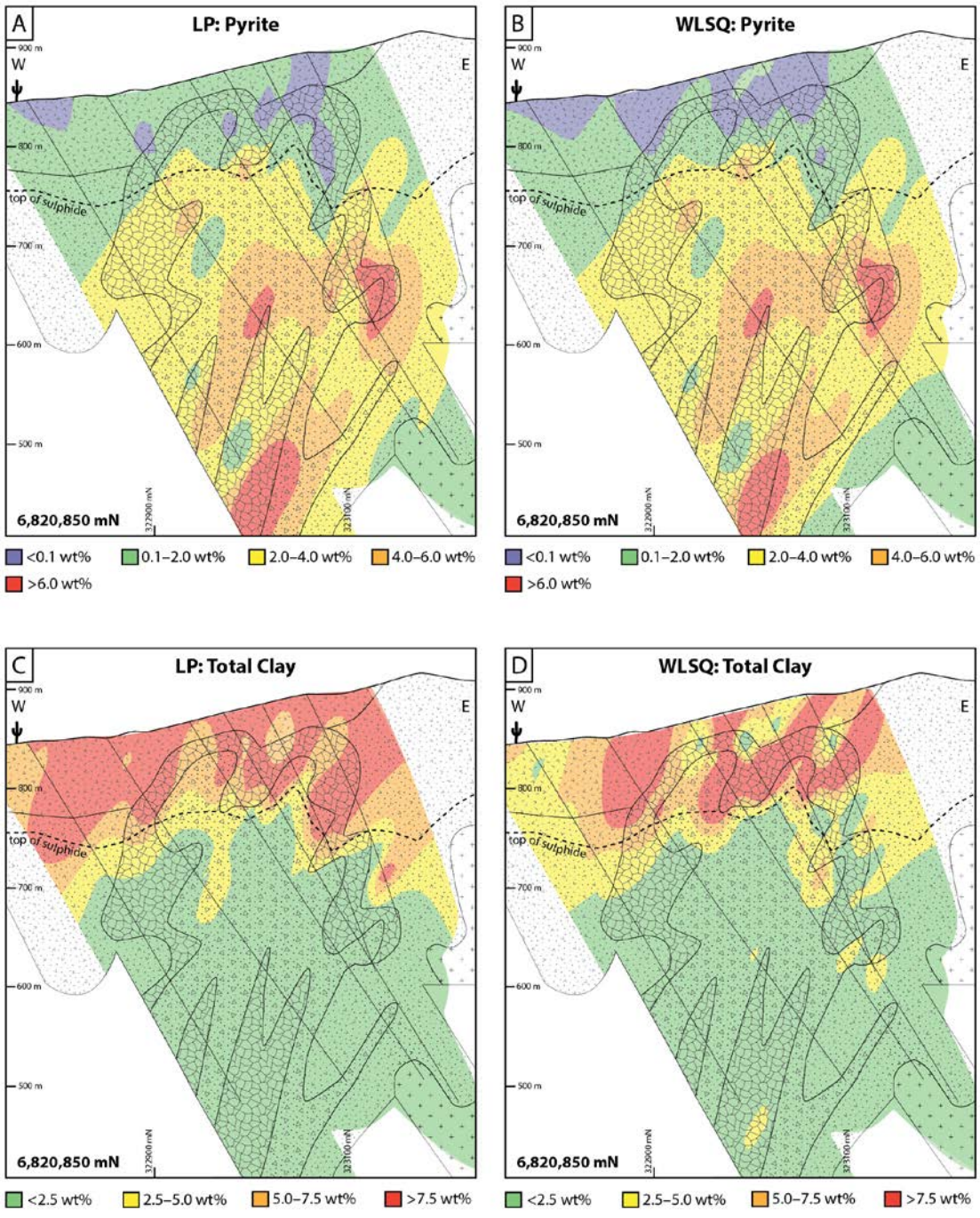

FIG 23. Plan slices at relative levels (RL) of 790, 730 and 680 m through 3D interpolant of calculated mineralogy by linear programming (LP) for A-C) total quartz and feldspar and D-E) total micas and chlorite. Interpolants generated in Leapfrog Geo version 3.1.0 (spheroidal interpolant; global trend with dip 75°, dip azimuth 285°, pitch 0; ellipsoid ratios maximum 2, intermediate 1, minimum 1; resolution 25). Black line = pit design (March, 2014). Dashed lines show study sections, 1 = 6,822,215 mN, 2 = 6,820,850 mN.

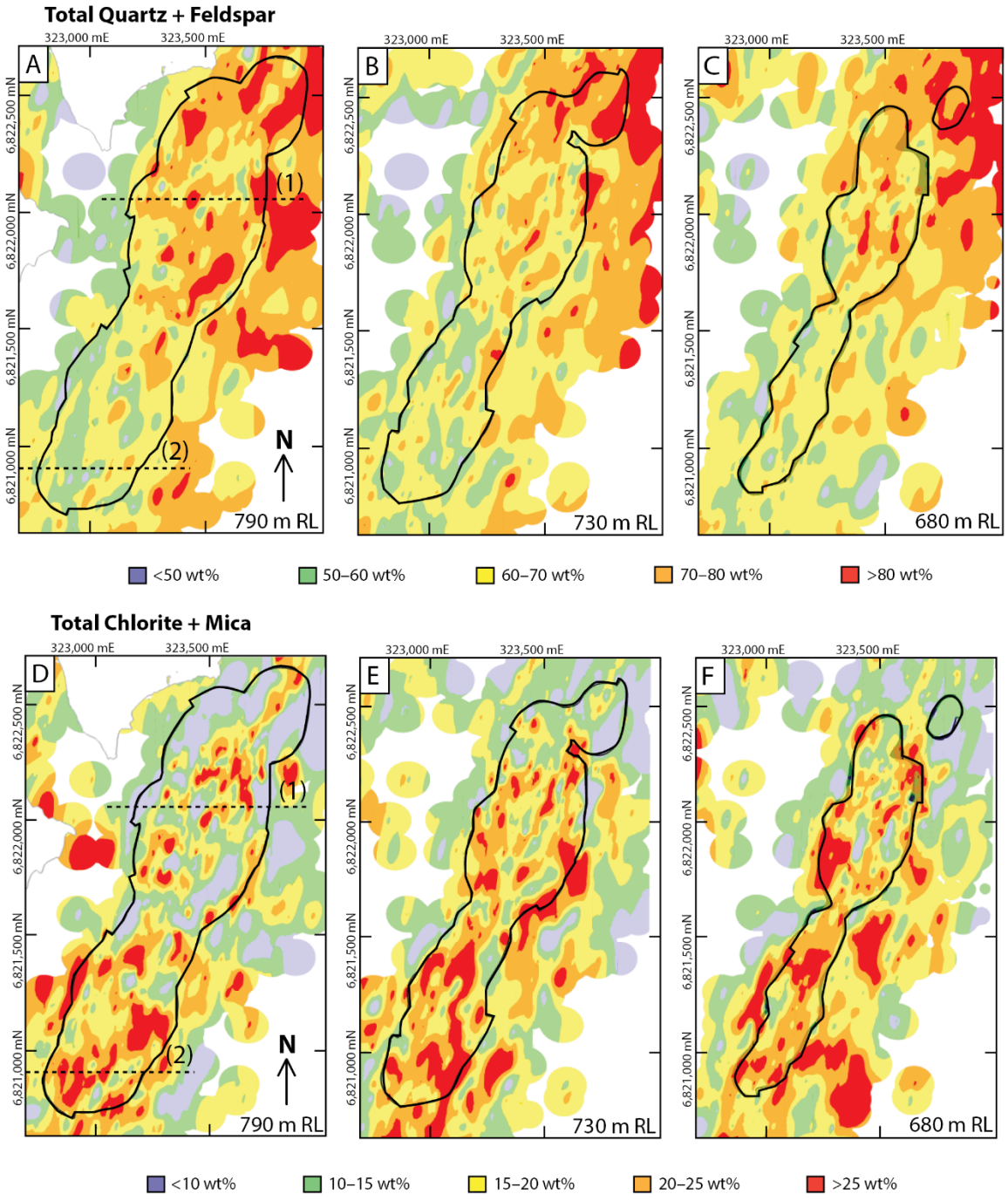

FIG 24. Plan slices at relative levels (RL) of 790, 730 and 680 m through 3D interpolant of calculated mineralogy by linear programming (LP) for A-C) pyrite and D-F) total clay. Interpolants generated in Leapfrog Geo version 3.1.0 (spheroidal interpolant; global trend with dip 75°, dip azimuth 285°, pitch 0; ellipsoid ratios maximum 2, intermediate 1, minimum 1; resolution 25). Black line = pit design (March, 2014). Dashed lines show study sections, 1 = 6,822,215 mN, 2 = 6,820,850 mN.